



On the effectiveness of nitrogen oxide reductions as a control over ammonium nitrate aerosol

S. E. Pusede^{1,a}, K. C. Duffey¹, A. A. Shusterman¹, A. Saleh¹, J. L. Laughner¹, P. J. Wooldridge¹, Q. Zhang², C. L. Parworth², H. Kim³, S. L. Capps⁴, L. C. Valin⁵, C. D. Cappa⁶, A. Fried⁷, J. Walega⁷, J. B. Nowak⁸, A. J. Weinheimer⁹, R. M. Hoff¹⁰, T. A. Berkoff¹¹, A. J. Beyersdorf¹¹, J. Olson¹¹, J. H. Crawford¹¹, and R. C. Cohen^{1,12}

¹Department of Chemistry, University of California Berkeley, Berkeley, CA 94720, USA

²Department of Environmental Toxicology, University of California at Davis, Davis, CA 95616, USA

³Center for Environment, Health and Welfare Research, Korea Institute of Science and Technology, Seoul, Korea

⁴Department of Mechanical Engineering, University of Colorado Boulder, Boulder, CO 80309, USA

⁵Lamont-Doherty Earth Observatory, Columbia University, Palisades, NY 10964, USA

⁶Department of Civil and Environmental Engineering, University of California at Davis, Davis, CA 95616, USA

⁷Institute of Arctic and Alpine Research, University of Colorado, Boulder, CO 80309, USA

⁸Aerodyne Research, Inc., Billerica, Billerica, MA 01821, USA

⁹Atmospheric Chemistry Division, National Center for Atmospheric Research, Boulder, CO 80307, USA

¹⁰Department of Physics, University of Maryland Baltimore County, Baltimore, MD 21250, USA

¹¹NASA Langley Research Center, Hampton, VA 23681, USA

¹²Department of Earth and Planetary Science, University of California Berkeley, Berkeley, CA 94720, USA

^anow at: Department of Environmental Sciences, University of Virginia, Charlottesville, VA 22904, USA

Correspondence to: Ronald C. Cohen (rccohen@berkeley.edu)

Received: 23 August 2015 – Published in Atmos. Chem. Phys. Discuss.: 7 October 2015

Revised: 17 February 2016 – Accepted: 18 February 2016 – Published: 2 March 2016

Abstract. Nitrogen oxides (NO_x) have fallen steadily across the US over the last 15 years. At the same time, NO_x concentrations decrease on weekends relative to weekdays, largely without co-occurring changes in other gas-phase emissions, due to patterns of diesel truck activities. These trends taken together provide two independent constraints on the role of NO_x in the nonlinear chemistry of atmospheric oxidation. In this context, we interpret interannual trends in wintertime ammonium nitrate (NH_4NO_3) in the San Joaquin Valley of California, a location with the worst aerosol pollution in the US and where a large portion of aerosol mass is NH_4NO_3 . Here, we show that NO_x reductions have simultaneously decreased nighttime and increased daytime NH_4NO_3 production over the last decade. We find a substantial decrease in NH_4NO_3 since 2000 and conclude that this decrease is due to reduced nitrate radical-initiated production at night in residual layers that are decoupled from fresh emissions at the surface. Further reductions in NO_x are imminent in California, and nationwide, and we make a quantitative prediction of the

response of NH_4NO_3 . We show that the combination of rapid chemical production and efficient NH_4NO_3 loss via deposition of gas-phase nitric acid implies that high aerosol days in cities in the San Joaquin Valley air basin are responsive to local changes in NO_x within those individual cities. Our calculations indicate that large decreases in NO_x in the future will not only lower wintertime NH_4NO_3 concentrations but also cause a transition in the dominant NH_4NO_3 source from nighttime to daytime chemistry.

1 Introduction

Aerosol abundances are decreasing across the US, improving air quality and affecting climate. These decreases have been broadly attributed to regulatory controls on the emissions of gas-phase precursors; however, it has proven difficult to link precursor reductions to observed changes in aerosol concen-

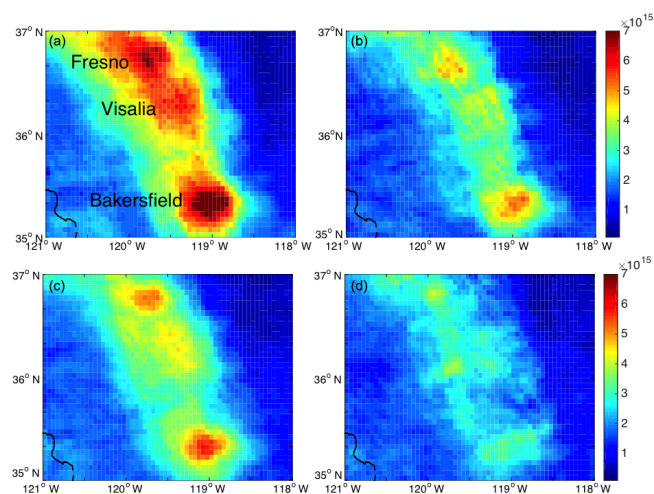


Figure 1. Wintertime (November–March) NO₂ columns (molecules cm⁻²) in the SJV using the UC Berkeley OMI BEHR retrieval (Russell et al., 2011). The urban NO₂ plumes of Fresno, Visalia, and Bakersfield are labeled to the left of their respective cities in panel (a). Panel (a) shows 2005–2006 weekdays (Tuesday–Friday). Panel (b) shows 2005–2006 weekends (Saturday–Sunday). Panel (c) shows 2012–2013 weekdays. Panel (d) shows 2012–2013 weekends.

tration via specific chemical mechanisms. Thus, there is limited knowledge of how impacts will scale in the future.

We present an analysis to identify driving chemical mechanisms and to quantify the effects of large reductions in nitrogen oxides (NO_x) (e.g., Russell et al., 2012; McDonald et al., 2012) on secondary aerosol chemistry. We take advantage of decreased NO_x emissions on weekends compared to weekdays, which occur mostly without changes in other gas-phase emissions (e.g., Dallmann et al., 2012), and couple these weekday–weekend patterns to long-term NO_x reductions (Pusede and Cohen, 2012). The effect is that weekday NO_x levels equal weekend NO_x years earlier in the record (Fig. 1). We use this NO_x constraint to interpret trends in observed wintertime ammonium nitrate (NH₄NO₃) concentrations over the last decade in the San Joaquin Valley (SJV) of California.

The SJV experiences the most severe aerosol pollution in the US (American Lung Association, 2014). From 2001 to 2013 there were on average 44 exceedances each winter (November–March) of the 24 h National Ambient Air Quality Standard (NAAQS) of 35 μg m⁻³ in the cities of Bakersfield and Fresno, with as many as 70 per winter early in the record. High aerosol in the SJV is generally limited to the winter months, with few exceedances occurring in other seasons. In the SJV, 30–80 % of wintertime aerosol mass is NH₄NO₃ and the remaining portion is mostly organic material (Chow et al., 2006; Chen et al., 2007; Ge et al., 2012). Characteristics of the wintertime SJV that are conducive to high aerosol abundances include shallow bound-

ary layers (Bianco et al., 2011); prolonged periods of stagnation (Smith et al., 1981); and large emissions of NO_x (NO_x ≡ NO + NO₂), ammonia (NH₃) (Goebes et al., 2003; Clarisse et al., 2010), and organic aerosol (Ge et al., 2012). These conditions pose challenges to accurately simulating secondary aerosol in the region, as models need to represent bidirectional NH₃ exchange (Gilliland et al., 2006; Flechard et al., 2010; Pleim et al., 2013), variable local meteorology, complex airflows, and vertical stratification in the rates of NO₂ oxidation to NO₃⁻ (Heald et al., 2012; Walker et al., 2012; Kelly et al., 2014; Schiferl et al., 2014; Markovic et al., 2014).

In this paper, we take an observational approach, combining the decade-long record of speciated aerosol concentrations and of gas-phase precursors in the region with detailed measurements collected during the DISCOVER-AQ experiment (Deriving Information on Surface Conditions from Column and VERTically resolved observations relevant to Air Quality, 14 January–14 February 2013). We show that wintertime NO₃⁻, which we treat as a measured surrogate for NH₄NO₃, has been dependent only on the NO₂ concentration over the last 12 years. We calculate observationally constrained nighttime and photochemical NO₃⁻ production rates and show that measured trends in wintertime NO₃⁻ can be explained by decreased nitrate radical-initiated production in nocturnal residual layers, which are unmonitored layers of the atmosphere that are effectively separated from surface emissions at night. We test the impacts of forthcoming NO_x emission controls on the probability of future NAAQS exceedances, showing that NO_x reductions will not only decrease the frequency of high aerosol days but also shift both the timing and the oxidation mechanisms that drive NH₄NO₃ production.

2 Results from observations

Trends in wintertime (November–March) 24 h NO₃⁻ versus daytime (10:00–15:00 local time) NO₂ are shown in Fig. 2 in the cities Fresno and Bakersfield on weekdays and weekends for the period 2001–2013. The source of these observations, the methods used for collection, and measurement biases are discussed in Appendix A. Weekdays are defined as Tuesday–Friday and weekends are Saturday–Sunday. We expect carryover to have an effect on the interpretation, as concentrations of NO₂ and aerosol are not only influenced by present day processes but also have some memory of processes occurring on the preceding day, especially in the winter when surface winds are slow and disorganized and horizontal transport is weak. We exclude Monday from weekdays for this reason but retain Saturdays to improve weekend statistics. As a result, weekend medians reported here might be slightly higher than would be observed due to weekend emissions alone. We define the day as beginning and ending at sunrise, since nighttime NO₃⁻ production builds from reac-

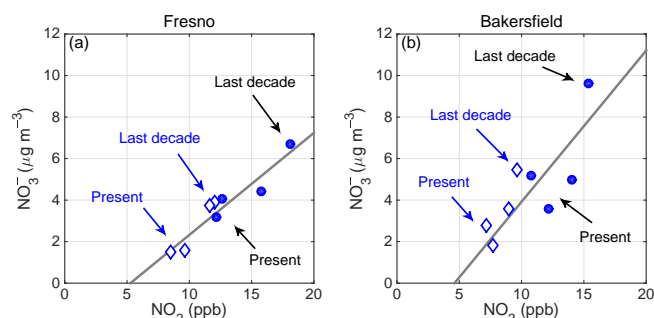


Figure 2. Observed NO_3^- ($\mu\text{g m}^{-3}$) in PM_{10} versus daytime (10:00–15:00 LT) NO_2 on weekdays (closed circles) and weekends (open diamonds). Data are 3-year medians of wintertime (November–March) data in Fresno (a) (2001–2012) and Bakersfield (b) (2001–2013). There are an average of 41 weekday days and 18 weekend days point⁻¹. Uncertainties in NO_3^- are $\pm 32\%$ $\mu\text{g m}^{-3}$ on weekdays and $\pm 40\%$ $\mu\text{g m}^{-3}$ on weekends for NO_3^- and less than $\pm 9\%$ on weekdays and $\pm 13\%$ on weekends for NO_2 (see text for details). Slopes are $0.5 \mu\text{g m}^{-3} \text{NO}_3^- \text{ppb}^{-1} \text{NO}_2$ in Fresno and $0.64 \mu\text{g m}^{-3} \text{NO}_3^- \text{ppb}^{-1} \text{NO}_2$ in Bakersfield and are calculated using a weighted linear least squares fit with errors assumed in both the x and y ; weights are computed as counting errors derived from the number of observations.

tants present in the atmosphere during the preceding daytime hours.

In the wintertime SJV, persistent stagnant conditions are common and punctuated only by infrequent cold fronts accompanied by strong winds that remove accumulated pollution from the basin. Stagnation events are a few days to multiple weeks in duration, and, during these stable periods, surface winds are slow and disorganized, controlled largely by surface heating, with limited horizontal mixing (Smith et al., 1981). On any individual winter day, air stagnation and planetary boundary layer height are the dominant controls over gas and aerosol concentrations; however, considering the data separately by weekday and weekend and then comparing year-to-year changes instead draws attention to the effects of emissions and subsequent chemistry.

By this method, the NO_3^- mass concentration is observed to have depended on the previous day's daytime NO_2 concentration with a sensitivity of $0.5 \mu\text{g m}^{-3} \text{ppb}^{-1} \text{NO}_2$ in Fresno and $0.64 \mu\text{g m}^{-3} \text{ppb}^{-1} \text{NO}_2$ in Bakersfield (slopes in Fig. 2). Uncertainties in the NO_3^- concentration are computed as counting errors, with N as the total number of wintertime data points (3-year average), and are $\pm 20\%$ on weekdays and $\pm 30\%$ on weekends. Errors in NO_2 are computed in the same way and are less than $\pm 9\%$ on weekdays and $\pm 13\%$ on weekends in both Fresno and Bakersfield. We interpret the positive x intercept in Fig. 2 as consistent with the known low bias in NO_3^- measurements (Appendix A) and the shorter wintertime atmospheric lifetime of NO_3^- than NO_2 (Sect. 4). Uncertainty estimates, including a low NO_3^-

measurement bias of 25 %, are $\pm 32\%$ $\mu\text{g m}^{-3} \text{ppb}^{-1} \text{NO}_2$ on weekdays and $\pm 40\%$ $\mu\text{g m}^{-3} \text{ppb}^{-1} \text{NO}_2$ on weekends. One ppb NO_2 corresponds to $2.56 \mu\text{g m}^{-3} \text{NO}_3^-$ after oxidation (at 25 °C and 1 atm); thus the observed correlation corresponds to a decrease in NO_3^- mass that is 20 % of the NO_2 decrease. While the full budget for wintertime NO_x loss is beyond the scope of this paper, Fig. 2 implies that on average in the wintertime, 20 % of each day's NO_x emissions are converted to NO_3^- in 1–2 days.

The key idea is that present-day NO_3^- concentrations on weekdays are equal to what were seen on weekends a decade ago, i.e., the NO_2 dependence of NO_3^- has been unchanged with time. This suggests that in the wintertime average, the only source of NO_3^- in the atmosphere has been oxidation of NO_2 and that NH_4NO_3 production has been nitrate rather than ammonium limited. Agreement of NO_3^- in different years at identical NO_2 implies that there has been little change over time in the chemical mechanism producing NO_3^- and hence NH_4NO_3 .

Additional evidence comes from observations made during DISCOVER-AQ, in which the sum of gas-phase nitric acid and aerosol-phase NO_3^- ($\text{NO}_3^-_{(\text{g+p})}$) was measured onboard the NASA P-3B on six research flights with almost identical flight patterns (Fig. 3a). See Appendix A for a description of the $\text{NO}_3^-_{(\text{g+p})}$ measurements and DISCOVER-AQ experiment. Comparing the spatial distribution of $\text{NO}_3^-_{(\text{g+p})}$ within the fully developed (afternoon) boundary layer (see Appendix A for the boundary layer filtering procedure) to NO_2 observed from the satellite (Fig. 1) and NO_x from onboard the P3-B (Fig. 3b) suggests that $\text{NO}_3^-_{(\text{g+p})}$ better follows spatial patterns in NO_2 than gas-phase NH_3 (Fig. 3c), the precursor of particulate-phase NH_4^+ .

In Fig. 3a, urban–rural gradients in $\text{NO}_3^-_{(\text{g+p})}$ are steep. In Bakersfield, $\text{NO}_3^-_{(\text{g+p})}$ was on average $18\text{--}20 \mu\text{g m}^{-3}$ near the city center, twice as high as just 20 km to the northeast. During DISCOVER-AQ, surface wind speeds were $\sim 2\text{--}3 \text{ m s}^{-1}$ in the daytime (10:00–15:00 LT), $\sim 1\text{--}2 \text{ m s}^{-1}$ in the morning (06:00–10:00 LT), and typically $< 1 \text{ m s}^{-1}$ at night. An air parcel moving within the surface layer at 3 m s^{-1} would require approximately ~ 20 daytime h, equivalent to multiple days, to either reach Fresno from the upwind cities of Stockton or San Jose or to reach Bakersfield from Fresno. An additional transport mechanism is mixing by winds in nocturnal low-level jets, which are well documented in the SJV in the summertime (Bao et al., 2008). There are few measurements of these winds in the winter, but wind speeds of up to $1\text{--}8 \text{ m s}^{-1}$ have been observed at 0.1–2 km a.g.l. (3 days of data), which are fast enough to mix species valley wide in 1–2 days (Chow et al., 2006). However, the measured spatial heterogeneity in $\text{NO}_3^-_{(\text{g+p})}$ (Fig. 3a) indicates faster and/or more localized processes control a significant portion of the NO_3^- concentration in each city.

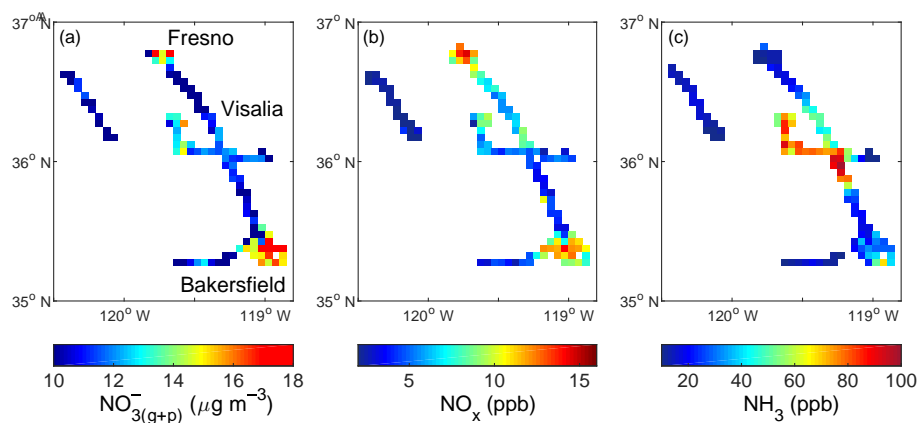


Figure 3. NO₃^{-(g+p)} (μg m⁻³) in PM_{2.5} (a), NO_x (ppb) (b), and NH₃ (ppb) (c) measured onboard the NASA P-3B below the fully formed afternoon boundary layer and at pressure altitude (a.s.l.) greater than 0 on the same days and averaged to a 0.05° × 0.05° grid.

We infer from Figs. 2 and 3 that the oxidation of locally emitted NO_x is the largest term affecting the production of NH₄NO₃, that NH₃ is in excess, and that transport and mixing are too slow to fully homogenize the aerosol throughout the wintertime SJV.

3 Chemistry in the dynamic near-surface atmosphere

Under the abundant NH₃, low sulfur dioxide, high aerosol, and low temperature conditions found in the wintertime SJV, most NO₃⁻ is aerosol bound in the 24 h average and NH₄NO₃ abundances are driven by NO₃⁻ production (*P*NO₃⁻). *P*NO₃⁻ occurs by distinct nighttime and daytime mechanisms, each of which is a nonlinear function of NO₂.

Nitrate radical (NO₃) is the most important nighttime oxidant (Brown and Stutz, 2012). It is formed via reaction of NO₂ with O₃ (Reaction 1).



NO₃-initiated chemistry occurs mainly at night because NO₃ photolyzes rapidly to NO₂. After sunset, large NO emissions can titrate O₃, altering the relative amounts of NO₂ and O₃ but conserving odd oxygen (O_x ≡ NO₂ + O₃). NO₃ radical production is a nonlinear function of NO₂ for a given O₃ concentration, increasing with NO₂ at low NO_x, maximizing when NO₂ is equal to O₃ at constant O_x, and decreasing at higher NO_x, shown as NO₂ (Appendix B, Fig. B1a).

In the evening, reduced sunlight diminishes the heating of the Earth's surface, leading to strong suppression of vertical mixing and the formation of a shallow nocturnal boundary layer (NBL). Between the NBL and the free troposphere, in the nocturnal residual layer (NRL), mixing is weak and further layering may occur (Brown et al., 2007). The initial concentrations of species in the NRL are determined by the concentrations observed at the point in time when the residual layer decouples from the NBL, around sunset. Af-

terwards, the strong surface inversion keeps fresh emissions from entering the NRL, yet vertical chemical gradients have been observed within layers (Brown et al., 2007). The NRL is seen by surface monitors in the morning when solar heating and turbulent mixing reincorporate what was the NRL into the growing daytime boundary layer (Fig. 4), a process that also alters the NRL composition. On nights when NO₃ radical production in the NBL is 0 due to high NO emissions, NO₃ chemistry may still be active in the dynamically decoupled NRL. Loss from the atmosphere is likewise affected by this vertical structuring, as deposition to the surface occurs during the daytime and during the night from the NBL but not during the night from the NRL. Figure 5 shows examples of enduring nocturnal structure seen via potential temperature, the vertical distribution of NO₃^{-(g+p)}, and O₃ during DISCOVER-AQ by the P-3B in the early mornings over Bakersfield. At least one NRL is apparent for each profile, evident in the potential temperature variability; however, due to a combination of extremely shallow surface inversions, intermittent NO₃^{-(g+p)} sampling, and science flight timing, it is unclear that the P-3B ever captured NO₃^{-(g+p)} concentrations in the NBL prior to the second flight circuit in the late morning (not shown) when significant atmospheric mixing had already taken place.

Nitrate radical reacts with NO₂ to form dinitrogen pentoxide (N₂O₅) and generally under atmospheric conditions of high NO₂ and low temperature, N₂O₅ ≫ NO₃ (Brown et al., 2009; Brown and Stutz, 2012). The lifetime of N₂O₅ to thermal decomposition to NO₂ and NO₃ is ~10 min at 270 K. NO₃ is also lost to reaction with certain organic species, especially compounds with unsaturated carbon-carbon bonds and aldehydes. When reaction times are long, for example during long, dark winter nights and when unsaturated hydrocarbon emissions are low, the most important loss of NO₃ is via N₂O₅ uptake onto aerosols (e.g., Dentener and Crutzen, 1993; Macintyre and Evans, 2010; Wagner et al., 2013),

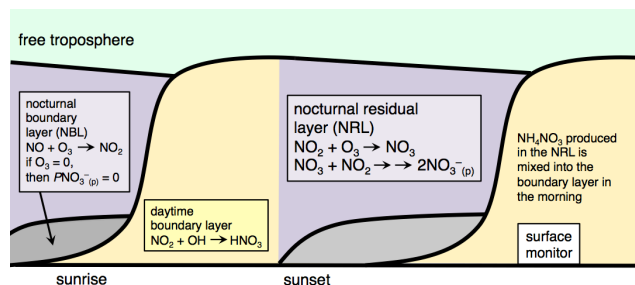
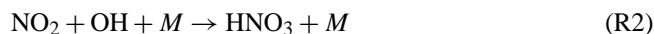


Figure 4. Simplified illustration of the diurnal evolution of the near-surface atmosphere as it relates to $P\text{NO}_3^-$. Boundary layer dynamics schematic adapted from Stull (1988).

whereupon N_2O_5 reacts with aerosol-phase water to give either two NO_3^- or, if NO_2^+ combines with Cl^- , $\text{ClNO}_2 + \text{NO}_3^-$. At sunrise, ClNO_2 photolyzes within a few hours (Nelson and Johnston, 1981), releasing NO_2 and Cl radical, the latter reacting rapidly with most gas-phase organic compounds. The heterogeneous loss rate of N_2O_5 is a function of the total aerosol surface area and of the fraction of gas-particle collisions resulting in N_2O_5 uptake. The latter is aerosol composition dependent, enhanced at higher aerosol water content (e.g., Hu and Abbatt, 1997; Hallquist et al., 2003; Thornton et al., 2003), reduced in the presence of organic coatings (e.g., Cosman and Bertram, 2008; McNeill et al., 2006), and inversely proportional to NO_3^- (e.g., Wahner et al., 1998; Hallquist et al., 2003; Bertram and Thornton, 2009; Wagner et al., 2013).

During the daytime, nitric acid (HNO_3) is the gas-phase reaction product of the oxidation of NO_2 and the hydroxyl radical (OH) (Reaction 2).



The production rate of HNO_3 increases rapidly with increasing NO_x at low NO_x and converges at a limit set by the primary HO_x ($\text{HO}_x \equiv \text{OH} + \text{HO}_2 + \text{RO}_2$) production rate at higher NO_x . Major sources of HO_x in the polluted troposphere are $\text{O}(^1\text{D}) + \text{H}_2\text{O}$, formaldehyde (CH_2O), and nitrous acid (HONO). The functional form of the dependence of HNO_3 production on NO_2 (Fig. B1b) arises from the nonlinear effects of NO_x on the OH abundance, as NO_x both propagates and terminates the HO_x catalytic cycle. Under the high NO_x conditions of the wintertime SJV, HNO_3 is the dominant daytime HO_x termination product. Combined with excess NH_3 , partitioning to the aerosol phase is a function of ambient temperature and humidity.

Trends in calculated wintertime $P\text{NO}_3^-$ for the nighttime and daytime mechanisms, as constrained by the observations (calculations and data are described in Appendix B), suggest that $P\text{NO}_3^-$ in the NRL is the largest source of chemistry that matches trends in NO_3^- (Fig. 2). Specifically, $P\text{NO}_3^-$ in the NRL exhibits identical NO_2 dependence as observed in the NO_3^- measurements – both over

time and from weekday to weekend. In Fig. 6, the calculated annual wintertime daily-integrated $P\text{NO}_3^-$ in the NRL is shown versus daytime NO_2 on weekdays and weekends in Fresno and Bakersfield. $P\text{NO}_3^-$ in the NRL has decreased by $0.9 \mu\text{g m}^{-3} \text{ day}^{-1} \text{ ppb}^{-1} \text{ NO}_2$ in both cities, a rate approximately twice the trend observed in NO_3^- versus NO_2 . The total daytime $P\text{NO}_3^-$ (Reaction R2), equal to the sum of $P\text{NO}_3^-$ attributed to the HO_x sources $\text{O}(^1\text{D}) + \text{H}_2\text{O}$, HONO , and CH_2O , has, by contrast, not significantly changed as a function of NO_2 over the last decade. In fact, $P\text{NO}_3^-$ linked to the HO_x sources $\text{O}(^1\text{D}) + \text{H}_2\text{O}$ and CH_2O has increased by $\sim 5\%$ since 2001. $P\text{NO}_3^-$ attributed to HONO has decreased since 2001 (Appendix B, Fig. B2), displaying comparable NO_2 dependence to both measured NO_3^- concentrations (Fig. 2) and calculated $P\text{NO}_3^-$ in the NRL (Fig. 6). However, we calculate that $P\text{NO}_3^-$ in the NRL is approximately 5 times greater than $P\text{NO}_3^-$ formed during the daytime from OH originating from HONO . In the NBL (not shown) $P\text{NO}_3^-$ has increased from < 1 to $3\text{--}5 \mu\text{g m}^{-3} \text{ day}^{-1}$ on weekdays and to $6\text{--}8 \mu\text{g m}^{-3} \text{ day}^{-1}$ on weekends due to reduced NO_x titration of O_3 at sunset. Increases in NBL $P\text{NO}_3^-$ are not reflected in Fig. 2, potentially because these changes have occurred within a small fraction of the volume of the NRL and daytime boundary layer and because depositional loss from the NBL is not impeded. For example, for an NBL that is 10% the NRL height, $P\text{NO}_3^-$ in the NBL would need to exceed 3 times the NRL production in order to alter the daytime boundary layer concentration by 20%, even if zero deposition is assumed.

4 Discussion

4.1 Relating concentration and $P\text{NO}_3^-$

The concentration of $\text{NO}_3^-_{(\text{g+p})}$ is a function of $P\text{NO}_3^-$, as well as loss and mixing. While high aerosol days in the SJV are in part attributed to persistent and severe stagnation, controls over the portion of aerosol mass that is NH_4NO_3 are more dynamic (e.g., Pandis and Seinfeld, 1990; Vayenas et al., 2005). In this section we show that the effects of loss and mixing on the NO_3^- concentration are consistent with observed NO_3^- trends over time, differences by day-of-week, accumulation rates during stagnation, and differences between Fresno and Bakersfield.

On days when NH_4NO_3 exceeded $20\text{--}30 \mu\text{g m}^{-3}$, typical during stagnation periods, the diurnal variability of surface NO_3^- was characterized by a steep and substantial increase in NO_3^- in the morning, a slow decline through midday, and a rapid decrease in the afternoon (Fig. 7). On these mornings, the rise rate of NO_3^- was consistent with two $P\text{NO}_3^-$ pathways: reincorporation of high- NO_3^- NRL air into the boundary layer and NO_3^- formed by daytime chemistry with HONO as the OH source. By contrast, OH -initiated produc-

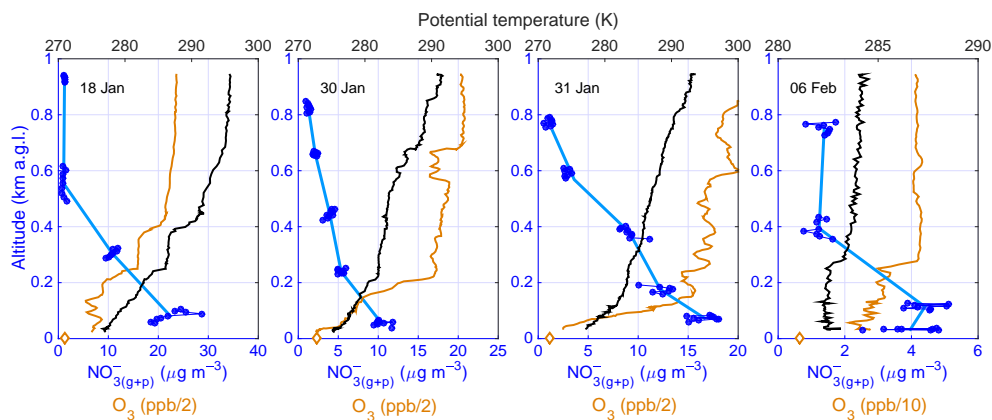


Figure 5. Vertical profiles of NO_3^- (g+p) ($\mu\text{g m}^{-3}$) in $\text{PM}_{2.5}$ between 08:00 and 09:00 LT over the city of Bakersfield on four flights when visibility and air traffic permitted a missed approach. Altitude data are in units km a.g.l. The O_3 (orange) and potential temperature (black) are also shown. The orange diamonds represent the mean O_3 measured at the surface (08:00–09:00 LT).

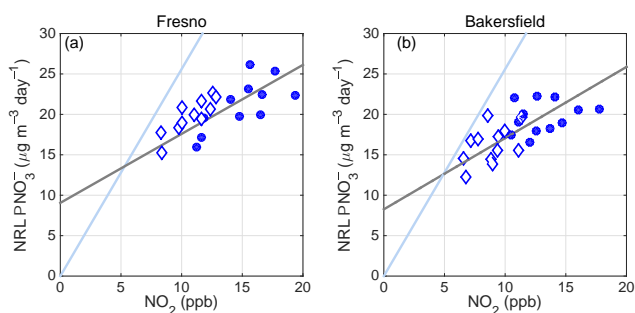


Figure 6. Calculated wintertime median PNO_3^- ($\mu\text{g m}^{-3} \text{ day}^{-1}$) in the NRL versus daytime (10:00–15:00 LT) NO_2 (ppb) in Fresno (a) and in Bakersfield (b). Calculations are shown separately for weekdays (closed circles) and weekends (open diamonds). Fresno and Bakersfield results include years 2001–2012 and 2001–2013, respectively. There was no significant difference between medians and means. The light blue line has a slope of 2.56, expected for unit conversion of NO_2 to NO_3^- (ppb to $\mu\text{g m}^{-3}$). The actual NO_3^- versus NO_2 slope (gray line) is calculated using a weighted linear least squares fit with errors assumed in both the x and y and weights that are the counting errors derived from the number of observations. The direction of time can be inferred from the NO_2 trends, as NO_2 concentrations have generally decreased each year over the decade.

tion attributed to $\text{O}(^1\text{D}) + \text{H}_2\text{O}$ and CH_2O increased gradually throughout the day. At midday, OH-initiated PNO_3^- , atmospheric loss, and mixing by winds all play upon $[\text{NO}_3^-]$. In the afternoon, OH-initiated PNO_3^- was minimal due to attenuated evening radiation. On days exhibiting this pattern, the NO_3^- concentration was observed to decrease at a rate equal to $3.0 \pm 1.3 \mu\text{g m}^{-3} \text{ h}^{-1}$ (1σ), with individual rates determined as the slopes of a linear fit through the magenta data and identified as periods of steady decrease at least three hours long. Time windows were allowed to vary and the average window was 13:25–16:05 LT, spanning 10:30–18:30 LT.

We use this afternoon rate of change, which is when loss dominates production and mixing, to derive the atmospheric NO_3^- lifetime ($\tau_{\text{NO}_3^-}$).

The atmospheric lifetime of aerosol in the boundary layer is determined by wet and dry deposition of aerosol, the wet and dry deposition of gases in equilibrium with aerosol, and mixing to the free troposphere where concentrations are much lower. Wet deposition occurs by interaction with rain, which scavenges aerosol and soluble gases, and leaves the valley relatively clear. Multi-day fog is common in the winter in the SJV (Holets and Swanson, 1981), enhancing NH_4NO_3 removal when fog leads to rain or drizzle (Jacob et al., 1986a, b), as inorganic ions readily partition into aqueous fog droplets (Waldman et al., 1982; Munger et al., 1983), but having little effect if fog dissipates. Fog has not been seen to accelerate the conversion of NO_2 to NO_3^- in the SJV (Jacob et al., 1984).

There are few direct measurements of deposition rates of aerosol, HNO_3 , and NH_3 . HNO_3 is theorized to deposit at a transport-limited rate, NH_3 exchange is dependent on surface and meteorological conditions, and aerosol, especially smaller particles, to deposit slowly. PM_{10} to $\text{PM}_{2.5}$ deposition velocities (v_d) have been reported to be 0.001 to 0.1 cm s^{-1} (Sehmel, 1980; Slinn, 1982; Farmer et al., 2013), too slow to account for the observed afternoon loss rates in Fig. 7. To compute NO_3^- loss by deposition of gas-phase HNO_3 , $\text{HNO}_{3(\text{g})}$ was modeled with ISORROPIA II (Nenes et al., 1998; Fountoukis and Nenes, 2007) run in forward mode, an approximation that was reasonable because during the wintertime temperatures were low, humidities were high, and NH_3 was abundant. ISORROPIA II was initialized as $[\text{NO}_3^- + \text{HNO}_3] = [\text{NO}_3^-]_{\text{AMS}}$ and $[\text{NH}_4^+ + \text{NH}_3] = [\text{NH}_4^+]_{\text{AMS}}$. Calculated $\text{HNO}_{3(\text{g})}$ was added back to $[\text{NO}_3^- + \text{HNO}_3]$, while $\text{NH}_{3(\text{g})}$ was added as 1.1 $\text{HNO}_{3(\text{g})}$ (by mole) to ensure NH_3 was in excess

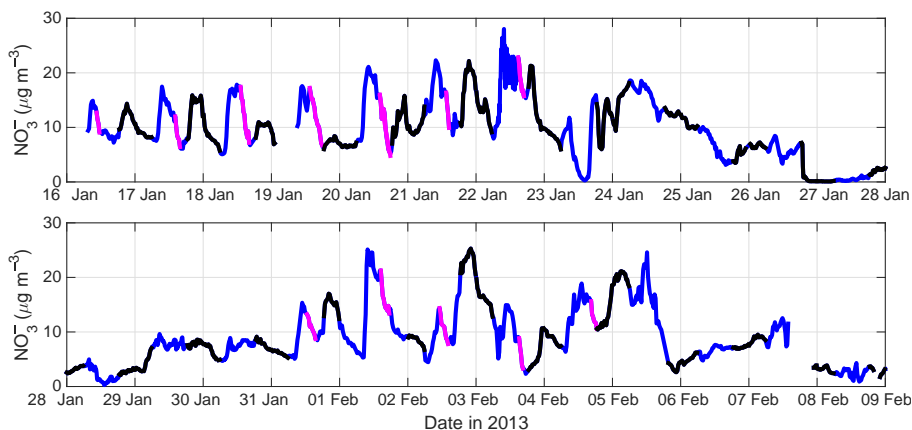


Figure 7. Time series of NO_3^- ($\mu\text{g m}^{-3}$) in PM_1 measured at the ground in Fresno during DISCOVER-AQ. Days are in blue and nights are in black. Select afternoon data (magenta) were fit to derive $\tau_{\text{NO}_3^-}$.

because we found NH_4NO_3 to be NO_3^- limited (Figs. 2 and 3). ISORROPIA II was solved iteratively until daytime $\text{HNO}_{3(\text{g})}$ changed by $< 2\%$ by mass. The phase state was set as metastable (e.g., Rood et al., 1989; Zhang et al., 2003; Vayenas et al., 2005). We assume that gases and aerosol are in equilibrium, that aerosols are homogenous and internally mixed, and that unaccounted-for factors do not influence the thermodynamics of the system (Vayenas et al., 2005). Calculated $\text{HNO}_{3(\text{g})}$ mixing ratios were greatest in the afternoon (12:00–16:00 LT), at which time they were 2 ppb on average for the DISCOVER-AQ time period and up to 4–6 ppb on the warmest days only. In the 24 h average, $\text{HNO}_{3(\text{g})}$ was 15 % of $[\text{NO}_3^- + \text{HNO}_3]$ by mass and was 40 % (median) in the afternoon. High $\text{HNO}_{3(\text{g})}$ was generally simultaneous with the magenta-highlighted NO_3^- data (Fig. 7). To compute the v_d of HNO_3 , the equation $\frac{\partial \text{NO}_3^-}{\partial t} = \frac{v_d}{h} C$ was solved, with $\frac{\partial \text{NO}_3^-}{\partial t}$ equal to the observed afternoon loss rate on designated (magenta) days, C equal to the daily mean $\text{HNO}_{3(\text{g})}$ over the same time windows, and h equal to the maximum boundary layer height (i.e., the afternoon height) visually identified according to aerosol backscatter estimates by a micro-pulse lidar (MPL) supplemented with a wide-field receiver system (Appendix A). In this way, we derived v_d equal to $5 \pm 2 \text{ cm s}^{-1}$, in line with previous direct measurements of $1\text{--}10 \text{ cm s}^{-1}$ (e.g., Huebert and Robert, 1985; Meyers et al., 1989; Sievering et al., 2001; Volpe Horii et al., 2005; Farmer et al., 2006) and constrained estimates of 6 cm s^{-1} (Vayenas et al., 2005). Given a v_d of 5 cm s^{-1} (assumed constant), the hourly $\frac{\partial \text{NO}_3^-}{\partial t}$ was computed for every hour of the day, with C equal to the time-varying $\text{HNO}_{3(\text{g})}$ and h equal to the time-varying boundary layer height. We assume losses are from the entire boundary layer, see Appendix C for our reasoning. For the daily time-varying h : the NBL was estimated as 10 % of the maximum daytime boundary layer height measured by MPL; the morning increase was estimated as linear over 5 h

and fully developed at 11:00; and the evening (18:00) collapse (also linear) was estimated as occurring in 2 h.

In this way and with respect to surface deposition alone, $\tau_{\text{NO}_3^-}$ was calculated to be 3 h (0.1 days) under daytime conditions. As a lower bound, if the true v_d was at the slowest end of previous observations (1 cm s^{-1}), then $\tau_{\text{NO}_3^-}$ would be 14 h under daytime conditions. Lifetimes in this range are shorter than typical stagnation periods, observed to be 5 ± 1.5 days (1σ) in both Fresno and Bakersfield (decadal average). By comparison, $\text{PM}_1\text{--PM}_{2.5} v_d$ yield $\tau_{\text{NO}_3^-}$ of 6–58 days. Such long lifetimes indicate the frequency of frontal passages controls the PM lifetime. Because the loss of NH_4NO_3 via HNO_3 deposition is rapid and PNO_3^- is relatively large, high aerosol days are expected to be more responsive to changes in emissions than expected when considering loss only through particle deposition.

There are other observational constraints that an account of aerosol NO_3^- in the SJV should explain. Median NO_3^- (2001–2013) is 25 % higher in Bakersfield than Fresno (Fig. 2). However, the observationally constrained calculated total PNO_3^- (NRL plus OH-initiated) is 15 % lower in Bakersfield than Fresno (Fig. 6). We find that wintertime stagnation events, defined as continuous days with increasing 24 h $\text{PM}_{2.5}$, are more severe in Bakersfield than in Fresno, meaning there is a greater increase in $\text{PM}_{2.5} \text{ day}^{-1}$ over each event. The median increase in $\text{PM}_{2.5} \text{ day}^{-1} \text{ event}^{-1}$ over the last decade was 15 % greater in Bakersfield ($7.9 \mu\text{g m}^{-3} \text{ day}^{-1} \text{ event}^{-1}$) than Fresno ($6.7 \mu\text{g m}^{-3} \text{ day}^{-1} \text{ event}^{-1}$) leading to 23 % larger increases in $\text{PM}_{2.5} \text{ event}^{-1}$ in Bakersfield ($32.5 \mu\text{g m}^{-3} \text{ event}^{-1}$) than Fresno ($25.1 \mu\text{g m}^{-3} \text{ event}^{-1}$). $\text{PM}_{2.5}$ on the first day of the event was also 20 % higher in Bakersfield ($8.6 \mu\text{g m}^{-3} \text{ event}^{-1}$ versus $6.9 \mu\text{g m}^{-3} \text{ event}^{-1}$). These differences between Bakersfield and Fresno may in part be attributed to the former's location in the southern end of the SJV, where the city is enclosed on three sides by the moun-

tains, resulting in reduced losses to advection and mixing than in Fresno. Likewise, transport may carry a portion of aerosol produced elsewhere in the valley to Bakersfield, either by advection in the surface-mixed layer or by a nocturnal low-level jet. Weaker correlations (r^2) in Fig. 2 in Bakersfield (0.6) than in Fresno (0.9) serve as evidence for enhanced influences of mixing and transport processes over NO_3^- concentrations in the southern SJV.

4.2 Impacts of future NO_x reductions

California has committed to additional, sizable controls on NO_x emissions, with decreases of at least 50 %, and potentially up to 75 % NO_x , imminent over the next decade. California has implemented a retrofit/replacement program to accelerate impacts of federal rules on diesel engines, affecting weekday NO_x (Dallmann and Harley, 2010; California Air Resources Board, 2012), and has both tightened standards on gasoline-powered vehicles and required one in seven new cars sold in the state be zero-emission or plug-in hybrids for model years 2017–2025 (Environmental Protection Agency, 2012), affecting weekday and weekend NO_x .

Currently, average wintertime NO_x concentrations are low enough that reductions of 50 and 75 % are calculated to decrease $P\text{NO}_3^-$ in the NRL in Bakersfield on weekends by 40 and 70 %, respectively (Fig. 8a), with similar results in Fresno and Visalia. Recall, the NO_3 radical production is nonlinear versus NO_2 and, for a fixed O_x concentration, production is described by a single curve in Fig. B1a. When O_x is variable, NO_3 radical production is described by multiple curves and is most sensitive to changes in O_3 at NO_2 concentrations which are at and/or greater than peak NO_3 radical production. At low NO_x (and high NO_x), $P\text{NO}_3^-$ that is limited by NO_3 radical production is more sensitive to changes in NO_2 . Figure 6 suggests that as a direct result of decreases in NO_2 , the chemical sensitivity of $P\text{NO}_3^-$ to NO_2 has been altered such that future NO_x controls are poised to more effectively slow $P\text{NO}_3^-$ in the NRL in the next decade than over the last, at least at weekend NO_x levels.

We compute that NO_x reductions of 50 and 75 % are large enough that changes in the average wintertime NO_3^- are quantified via 2.56 : 1 line (3.31 including molar equivalent NH_4^+), the stoichiometric NO_3^- response to NO_2 , meaning the O_3 feedback from reduced NO_x on $P\text{NO}_3^-$ is minimal. The highest NO_x conditions in the SJV are present in the shallowest boundary layers of December and January; during DISCOVER-AQ, NO_x concentrations were high enough that reduced weekend NO_x (21–22 January) had the effect of increasing $P\text{NO}_3^-$ in the NRL relative to the preceding weekdays, i.e., chemistry on these days was right of peak NO_3 radical production.

Our calculation implies greater decreases in $P\text{NO}_3^-$ have occurred in lower- NO_x rural environments than in cities since 2001 given the same relative NO_x reductions. During a previous aerosol experiment, CRPAQS (California Regional

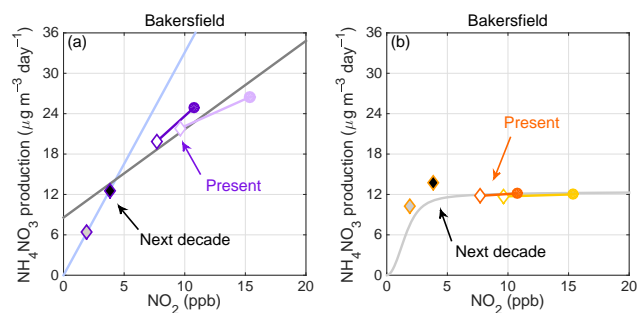


Figure 8. In Bakersfield: tethered 3-year weekday (closed circles) and weekend (open diamonds) medians of calculated wintertime NH_4NO_3 production ($\mu\text{g m}^{-3} \text{day}^{-1}$) in the NRL (a) and during the daytime (b) versus NO_2 . Medians and means give the same result. Brighter data are observationally constrained 3-year medians at present (2010–2013). Pale points are observationally constrained 3-year medians at the start of the record (2001–2004). Predicted NH_4NO_3 production at -50% weekend NO_x are black-filled diamonds and -75% weekend NO_x are gray-filled diamonds. Weekend data were selected simply to expand the NO_x range of individual curves; impacts on weekdays can be inferred. In panel (a), the light blue line is stoichiometric and the gray line is a fit to the annual observations as in Fig. 5. In panel (b), the gray line is the calculated HNO_3 production with $P\text{HO}_x$ and organic reactivity equal to present-day values.

$\text{PM}_{10}/\text{PM}_{2.5}$ Air Quality Study), conducted December 1999–February 2001 (Watson et al., 2000) with a wintertime intensive (15 December 2000–3 February 2001), it was generally observed that high NH_4NO_3 was a valley-wide phenomenon. CRPAQS measurements of 24 h NO_3^- (November 2000–January 2001) were similar in rural locations and in Fresno and Bakersfield, while high organic aerosol concentrations were spatially correlated with the cities. From these data, it was hypothesized that nocturnal low-level currents efficiently transported NH_4NO_3 and NO_3^- precursors, distributing NH_4NO_3 and NH_4NO_3 production throughout the SJV (Chow et al., 2006). On the contrary, during DISCOVER-AQ, NO_3^- was observed to spatially correlate with cities. Long-term co-located NO_3^- and NO_2 measurements do not exist at any rural location in the SJV; however, the discrepancy between spatial patterns during DISCOVER-AQ and during CRPAQS can be explained through a combination of NO_x emission controls shrinking urban NO_x plumes and low- NO_x nighttime chemistry being more sensitive to changes in NO_2 .

For NO_x emission changes to affect daytime $P\text{NO}_3^-$, they must be large enough to transition photochemistry into the NO_x -limited regime, less than a few ppb in the wintertime SJV (Fig. B1b). In Bakersfield (Fig. 8b), at -50% NO_x from current levels we predict an increase in daytime NH_4NO_3 production of $2 \mu\text{g m}^{-3} \text{day}^{-1}$ ($\sim 15\%$), but at -75% NO_x , we predict a transition to low- NO_x chemistry and a net decrease in NH_4NO_3 production of $1.5 \mu\text{g m}^{-3} \text{day}^{-1}$ (15%).

Initial enhancements in NH₄NO₃ are caused by NO_x feedbacks on the HO_x precursors, O₃ and CH₂O, which are both predicted to increase in response to decreases in NO₂ (Fig. B2). In Fig. 7b, the gray line is the modeled NH₄NO₃ production day⁻¹ calculated for present day conditions. The modeled points show the results of the calculations, for which the influence of NO_x decreases on PHO_x, and the subsequent feedbacks on NH₄NO₃ production, are accounted. Elevation of NH₄NO₃ production above the gray line is due to the NO₂-PHO_x precursor feedback. In Fresno (not shown), we compute an increase of 0.5 μg m⁻³ day⁻¹ (< 5 %) at -50 % NO_x and a decrease in NH₄NO₃ production of ~ 3 μg m⁻³ day⁻¹ (20 %) at -75 % NO_x.

Combining our derived trends in NRL and daytime PNO₃⁻ (Table 1), we calculate impacts of past and future NO_x controls on the frequency of wintertime 24 h PM_{2.5} NAAQS exceedances. Using data from a multi-year experiment in the early 2000s in Fresno (Appendix A), the 24 h NO₃⁻ concentration was observed to be an almost constant fraction of 24 h PM_{2.5} each winter when 24 h PM_{2.5} was greater than 15 μg m⁻³ and an even larger fraction at lower loadings, typically in March. During DISCOVER-AQ, surface aerosol in Fresno was 41 % (median) and 39 % (mean) NO₃⁻ in PM_{2.5}, and 57 % (median) and 53 % (mean) NH₄NO₃ in PM_{2.5}. Previous work has shown that NH₄NO₃ is a smaller portion of total PM_{2.5} in Fresno than in any other location in the SJV, including Bakersfield, with rural PM_{2.5} dominated by NH₄NO₃ (Zhang et al., 2010). We applied our calculated changes in PNO₃⁻ to 50 % of wintertime PM_{2.5} mass as a conservative estimate. We also assume that NH₄NO₃ has been and will continue to be 50 % of the aerosol mass over the entire past and future record. This simplification implies there have and will be only small changes in the heterogeneous loss rate of N₂O₅, in the relative speciated NO₃ reactivity, and in the fractional product yields of N₂O₅ hydrolysis. Figure 2 suggests these factors have not substantially affected the NO₂ dependence of NO₃⁻ over time, at least in the wintertime average in this location. We find that over the last decade, the impact of NO_x controls on PNO₃⁻, and hence NH₄NO₃, has been to reduce the number of 24 h PM_{2.5} exceedances by 18–46 % (Table 1). The primary mechanism for these changes has been decreased PNO₃⁻ in the NRL. Trends in PO₃⁻ account for 32–90 % of the total observed change. We hypothesize that controls on the organic portion of aerosol mass, for example district-level amendments to national home wood burning and fireplace rules (San Joaquin Valley Air Pollution Control Board, 2003), may have driven the other portion of reductions.

In the future, a 50 % decrease in NO_x is predicted to decrease PNO₃⁻ in the NRL more efficiently and to the point where this source is approximately equal to OH-initiated PNO₃⁻ on weekends. If reductions of 75 % NO_x are achieved, PNO₃⁻ in the NRL will decrease sufficiently that daytime OH-initiated HNO₃ formation is anticipated to

become the dominant source of wintertime NH₄NO₃ on all days of the week. We calculate that over the next decade the SJV will experience 7–16 % fewer exceedance days with a 50 % decrease in NO_x and ~ 30 % fewer exceedances with a 75 % decrease in NO_x.

We have not considered the impact of NH₃ controls because our data indicate PNO₃⁻ chemistry, not the NH₃ abundance, drives NH₄NO₃ (Figs. 2 and 3), and because it has been shown that NH₃ emissions in the SJV are too high for any reasonable NH₃ control to affect wintertime NH₄NO₃ concentrations (Herner et al., 2006). While these NO_x controls constitute a major improvement to the air quality in the SJV, it is evident that decreases in organic aerosol mass are also required to eliminate high aerosol days in the SJV. We have not quantified, but do expect, future NO_x reductions to influence the production of secondary organic aerosol (SOA) mass. In the laboratory, it has consistently been observed that NO_x concentrations, relative to gas-phase organic compounds, influence the molecular identity and volatility of oxidation products such that SOA yields are higher at low NO_x and suppressed at high NO_x (e.g., Presto et al., 2005; Ng et al., 2007; Kroll and Seinfeld, 2008; Chan et al., 2010). Recent summertime field measurements of aerosol-phase RONO₂ in Bakersfield (Rollins et al., 2012) and at a forested field site in Colorado (Fry et al., 2013) found that NO₃ radical-initiated SOA formation correlated with NO₃ production and was proportional to NO_x at low to moderate NO_x levels. In Fresno during DISCOVER-AQ, SOA constituted 40 % of the organic fraction of PM₁, or 22 % of total PM₁ mass (Young et al., 2015). Reductions in NO_x as large as 50 to 75 % are expected to influence this portion of the aerosol mass and likely in a way that affects the frequency of exceedances in the SJV; however, the magnitude and sign of the impact are beyond the scope of this work.

Additional benefits of NO_x decreases include reductions in high summertime O₃ throughout the SJV (Pusede and Cohen, 2012; Pusede et al., 2014) and decreases in both summertime inorganic nitrate aerosol (Markovic et al., 2014) and NO₃-radical initiated SOA (Rollins et al., 2012). Because the US EPA has recently decided to strengthen the annual PM_{2.5} standard of 12 μg m⁻³ (Environmental Protection Agency, 2013), compliance with this NAAQS in the SJV will require reductions in aerosol concentrations in all seasons. Generally speaking, regulatory policies of valley-wide inter-pollutant trading of NO_x for PM_{2.5} control aimed at wintertime NH₄NO₃ must be designed with knowledge of each nonlinear PNO₃⁻ mechanism versus NO₂, instead of use of a single exchange rate, as urban (high-NO_x) and rural (low-NO_x) PNO₃⁻ are differently responsive to changes in NO₂. Finally, because NO₃⁻ is concentrated over Fresno and Bakersfield, NO_x reductions need to happen in those cities themselves, prioritizing localized interventions to maximize the public health benefit and probability of regulatory compliance.

Table 1. Effects of three NO_x emission control scenarios on wintertime 24 h PM_{2.5} NAAQS exceedances in Fresno, Visalia, and Bakersfield. Percentages are calculated according to days in which data exist, not total wintertime days. Rows 1–2: average exceedances winter⁻¹ (November–March) in the last 3 years of the record, rounded up, and percentage of days in violation. Rows 3–9: number of exceedances predicted after a 50 % increase (back in time) and 50 and 75 % reductions in NO_x, including the calculated percent change from present day. In row 3, the number in parentheses is the actual number of exceedances averaged for 2001–2004. In row 5, the number of calculated exceedances was rounded down to compute the percent.

Control	Fresno	Visalia	Bakersfield
Exceedances (winter ⁻¹)	34	21	34
Winter days in exceedance (%)	31	14	23
+50 % NO _x			
Exceedances after the control (winter ⁻¹)	48 (60)	31 (31)	40 (53)
% change in exceedances	40	46	18
% change explained by the NO _x reduction	50	90	32
-50 % NO _x			
Exceedances after the control (winter ⁻¹)	32	19	29
% change in exceedances	-7	-10	-16
-75 % NO _x			
Exceedances after the control (winter ⁻¹)	24	16	24
% change in exceedances	-31	-27	-32

5 Conclusions

We derived trends in the wintertime production of NO₃⁻ (PNO₃⁻) as calculated from measurements of gas-phase precursors over the last 13 years. We used these PNO₃⁻ trends to explain the observed NO₃⁻ sensitivity to NO₂, which was -0.5 and -0.64 μg m⁻³ ppb⁻¹ NO₂ in the San Joaquin Valley cities of Fresno in Bakersfield, respectively. We found that reductions in NO_x have both decreased and increased NH₄NO₃ formation rates by the various chemical pathways, but the net downward trend in NO₃⁻ has been driven by local changes in nighttime chemistry in residual layers decoupled from fresh surface emissions. We showed that high NH₄NO₃ abundances were a combined function of active chemical PNO₃⁻ and rapid atmospheric loss by deposition of gas-phase HNO₃ (τ_{NO₃⁻} ~ 3 daytime h); in contrast, the total aerosol mass lifetime was controlled by cold fronts that turnover valley air on average every 5 ± 1.5 days. We computed the impact of future NO_x decreases on PNO₃⁻ from both nighttime and daytime mechanisms, finding the sign and magnitude of the changes are dependent on oxidation pathway, oxidant precursor, NO₂ concentration, and, at night, altitude. We calculated that the SJV will experience 7–16 % fewer days in exceedance of the 24 h PM_{2.5} standard with a 50 % NO_x reduction and ~ 30 % fewer 24 h PM_{2.5} exceedance days with a 75 % NO_x reduction. As an additional consequence of anticipated NO_x controls, daytime rather than nighttime chemistry will drive NH₄NO₃ production in the SJV in the future. The observations and calculations presented here offer improved insight into the chem-

istry imbedded in the wintertime NH₄NO₃ diurnal cycles and suggest such long-term measurements would inform the absolute and relative contributions by vertically stratified NO₃ chemistry and OH-initiated production, especially if a record that captured diurnal variability were put in place prior to the sizable NO_x reductions that are forthcoming. The specific NO_x constraints on NH₄NO₃ chemistry we described here likely inform the effects of NO_x emission changes, both increases and decreases, on aerosol in other polluted cities.

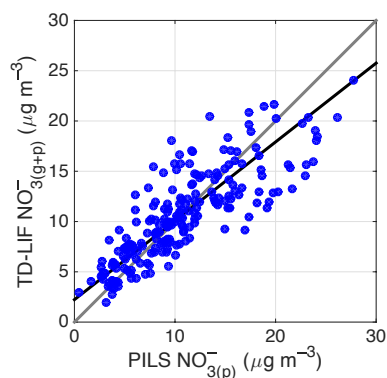


Figure A1. P-3B TD-LIF $\text{NO}_3^-(\text{g+p})$ in $\text{PM}_{2.5}$ versus PILS NO_3^- in PM_3 below 0.5 km a.s.l. The gray line is one-to-one and the black line is a least squares fit assuming equal weights in x and y data.

Appendix A: Measurements

A1 Long-term records

The long-term aerosol NO_3^- data are from 24 h integrated filter-based measurements of PM_{10} collected once every 3 to 6 days as part of the US EPA's Chemical Speciation Network program. The data were downloaded from the California Air Resources Board (CARB) archive (<http://www.arb.ca.gov/aqmis2/aqselect.php>). We used measurements at Fresno-First Street (36.782° N, 119.773° W) and Bakersfield-5558 California Avenue (35.357° N, 119.063° W), as the two stations had mostly uninterrupted records and co-located observations of NO_2 and O_3 . In Fig. 2, Bakersfield NO_3^- wintertime (November–March) medians include the years 2001–2013 with an average of 46 weekday and 18 weekend data points year⁻¹. The Fresno-First Street station was closed in 2012 and so the Fresno NO_3^- wintertime medians include 2001–2012 with an average of 36 weekday and 17 weekend data points year⁻¹.

To make these NO_3^- measurements, ambient air is sampled through a denuder and aerosol are collected on a quartz fiber filter for 24 h, midnight to midnight. Water-soluble ions are then quantified by ion chromatography. NH_4NO_3 is semi-volatile and exists in thermal equilibrium with gas-phase HNO_3 and NH_3 . Long sample collection times (24 h) and the presence of a denuder result in low biases due to loss of NO_3^- to the gas phase (Appel et al., 1981; Shaw Jr. et al., 1982; Hering and Cass 1999; Babich et al., 2000). This interference is well documented and observed to be large during summer months, when more than 80 % of NH_4NO_3 may be lost, but is estimated to be $\sim 20\%$ when relative humidities are high and temperatures are cold (Appel et al., 1981; Shaw Jr. et al., 1982; Hering and Cass, 1999). If we assume ambient conditions, as opposed to conditions internal to the instrument, drive the equilibrium (Appel et al., 1981; Shaw Jr. et al., 1982; Hering and Cass, 1999;

Babich et al., 2000), we are able to estimate the interference using surface AMS observations of NO_3^- , NH_4^+ , Cl^- , and sulfate (SO_4^{2-}) and a particle into liquid sampler (PILS) of potassium (K^+) and magnesium (Mg^+) in Fresno during DISCOVER-AQ to constrain the thermodynamic model ISORROPIA II (Nenes et al., 1998; Fountoukis and Nenes, 2007). To do this, we set the total gas plus particle concentration equal to the ion data, running ISORROPIA II in the forward mode to simulate the gas–aerosol partitioning after the air stream passed through a denuder, consistent with all gases being captured by the denuder and all aerosol depositing on the filter. During DISCOVER-AQ, the daily average temperature and relative humidity (RH) were 8.5 °C and 70 %, respectively. Median daytime (08:00–18:00) wintertime temperatures were within $\sim 1^\circ\text{C}$ and 1 % RH in Bakersfield and Fresno. When these conditions drive the interference, we predict that daily-integrated NO_3^- was biased low by 25 %, in line with other reports (Chow et al., 2005). The average wintertime (November–March) temperature and RH at the USDA Shafter Station from 2000 to 2013 were 10 °C and 79 %, respectively. Under these ambient conditions, we predict measurements of the daily-integrated NO_3^- are biased low by 23 %. Evaporative loss of NO_3^- of 25 % implies the true slope is 20 % greater with respect to the measured value. The observed correlation between NO_3^- and NO_2 indicates $\sim 20\%$ of NO_2 is oxidized to NO_3^- (Fig. 2), a 20 % NO_3^- error implies that 25 % of NO_2 is oxidized to NO_3^- .

Hourly O_3 , 24 h total $\text{PM}_{2.5}$, and NO_2 data are from the CARB archive at the following sites: Fresno-First Street (2000–2011), Fresno-Garland (36.785° N, 119.773° W) (2011–2013), Visalia-North Church Street (36.333° N, 119.291° W) (2000–2013), and Bakersfield-5558 California Avenue (2000–2013). NO_2 measurements are made by chemiluminescence coupled to a heated molybdenum catalyst and have a known but poorly quantified positive interference from higher oxides of nitrogen (Winer et al., 1974; Williams et al., 1998; Dunlea et al., 2007). This interference is largest in the summertime when weakly bound higher oxides are more abundant relative to NO_x and minimal in the wintertime. These instruments sample ambient air through a filter, removing NO_3^- and likely a considerable fraction of gas-phase HNO_3 and multifunctional organic nitrates, reducing the positive artifact. NO_2 concentrations are decreasing across the valley at a rate similar to that observed from space by OMI, an instrument selective for NO_2 , suggesting that relative trends in NO_2 are accurate (Russell et al., 2010).

Hourly solar radiation, temperature, and RH data were taken from the California Irrigation Management Information System archive (<http://www.cimis.water.ca.gov>) at the Shafter US Department of Agriculture (USDA) station (35.530° N, 119.280° W). Sunrise and sunset times in Bakersfield (35.357° N, 119.063° W) were downloaded from the

Table A1. Species, measurement accuracy, analytical technique, time resolution, location/platform, and reference for select DISCOVER-AQ observation included in our analysis. Many compounds are measured with higher precision than accuracy. See original references for details.

Species	Accuracy ($\pm\%$)	Analytical technique	Resolution	Location	Reference(s)
NO_3^- (g+p)	20	TD-LIF	1 s	P-3B	Day et al. (2002)
PM_{10} ions	20	AMS	20 min	Fresno-Garland	Drewnick et al. (2005); Ge et al. (2012)
$\text{PM}_{2.5}$ ions	20	PILS	20 min	Fresno-Garland	
NO_2	5	LIF	1 s	P-3B	Thornton et al. (1999)
NH_3	35	cavity ring down	8–20 s	P-3B	Picarro G2103 analyzer
CH_2O	4	IR absorption	1 s	P-3B	Weibring et al. (2006, 2007)

United States Naval Observatory Naval Oceanography Portal (http://aa.usno.navy.mil/data/docs/RS_OneYear.php).

Nitrate ion observations with 10 min time resolution were available during select time periods and were used to determine the wintertime variability in the fraction of $\text{PM}_{2.5}$ that was NO_3^- . These data were collected in Fresno in 2000–2001 and 2003–2005 (Watson et al., 2000) as part of the EPA PM Supersites program (<http://www.epa.gov/ttnamti1/supersites.html>). These measurements were made by flash volatilizing NH_4NO_3 , reducing HNO_3 across a heated catalyst to nitric oxide (NO), and detecting NO by chemiluminescence (Stolzenburg et al., 2003; Chow et al., 2008). It was reported that 24 h averages of these high-time-resolution observations were well correlated with, but 20–40 % lower than, 24 h $\text{PM}_{2.5}$ filter samples (annual averages). This effect has been attributed to incomplete volatilization and/or incomplete catalytic conversion of NO_3^- to NO. Two identical instruments at the Fresno supersite yielded data that were also well correlated but different by 10–55 % in the annual average (Chow et al., 2008). As a result, we treat these observations as uncalibrated but internally consistent over time.

A2 DISCOVER-AQ observations

The DISCOVER-AQ experiment synchronized multiple ground sites and aircraft sampling of in situ and column measurements, producing a data set resolved in space, both horizontally and vertically, and in time. The DISCOVER-AQ sampling strategy was built on repeated sampling across urban–rural (horizontal) and vertical gradients and on connecting observations made from balloons, onboard aircraft, and from space to monitoring sites at the surface. The NASA P-3B aircraft flew only during daylight hours, completing 2–3 identical circuits day⁻¹, alternating low-altitude (150 m a.g.l.), along the valley's western edge, medium-low (300 m a.g.l.), and high-altitude flight passes (2.6 km a.g.l.). Circuits included missed approaches at all cities and rural waypoints when visibility permitted. Missed approaches allowed the P-3B to reach altitudes as low as 20–40 m (a.g.l.) and were conducted over airstrips. Landing strips were often rural and little trafficked but may have experienced airport-related NO_x enhancements in the cities of Fresno and Bakersfield.

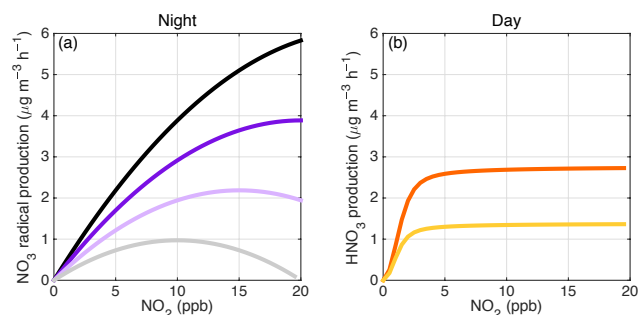


Figure A2. Panel (a): nighttime NO_3 radical production ($\mu\text{g m}^{-3} \text{h}^{-1}$) versus NO_2 (ppb) under four O_x conditions: 50 ppb O_x (black), 40 ppb O_x (purple), 30 ppb O_x (violet), and 20 ppb O_x (gray). The temperature is 282 K and NO_3 radical production is scaled by two, i.e., all NO_3 reacts with NO_2 and N_2O_5 hydrolysis is rapid compared to NO_3 formation. Panel (b): daytime production of HNO_3 ($\mu\text{g m}^{-3} \text{h}^{-1}$) as a function of NO_2 computed with an analytical model at $\text{NO}:\text{NO}_x = 0.3$ and $\text{VOCR} = 4 \text{ s}^{-1}$ at 0.3 ppt s^{-1} PHO_x (orange) and 0.15 ppt s^{-1} PHO_x (golden).

The comprehensive suite of DISCOVER-AQ data is available to the public at <https://www-air.larc.nasa.gov/cgi-bin/ArcView/discover-aq.ca-2013>. Table A1 lists the measurement accuracy, analytical technique, platform and location, and associated references of species key to this analysis.

The NO_3^- (g+p) measurements were made by thermal dissociation laser induced fluorescence (TD-LIF). The TD-LIF operating principle is as follows: NO_2 is detected by laser-induced fluorescence (LIF) (Thornton et al., 1999). A tunable dye laser is pumped by a Q-switched, frequency doubled $\text{Nd}^{3+}:\text{YAG}$ laser. The narrow band dye laser is etalon-tuned to a specific 585 nm rovibronic feature of NO_2 , alternating between this feature and the weaker continuum absorption. The resulting red-shifted photons are imaged onto a photomultiplier tube and collected using time-gated counting. The LIF technique is spectroscopically specific and accurate ($\pm 5\%$). The system was calibrated in flight every ~ 30 min with an NO_2 reference standard added at the inlet. The higher oxides of nitrogen, peroxy nitrates (RO_2NO_2), alkyl nitrates (RONO_2), and HNO_3 were measured by thermal dissociation (TD) coupled to LIF (Day et al., 2002).

Dissociation of thermally labile species into NO_2 and a companion radical occurs at characteristic temperatures due to differing N–O bond strengths. Ambient air is pulled through heated quartz tube ovens followed by PFA sampling lines before reaching the NO_2 detection cell. An unheated channel detects only NO_2 , a second channel (180°C) measures $\text{NO}_2 + \text{RO}_2\text{NO}_2$, a third channel (400°C) measures $\text{NO}_2 + \text{RO}_2\text{NO}_2 + \text{RONO}_{2(\text{g+p})}$, and a fourth (600°C) measures $\text{NO}_2 + \text{RO}_2\text{NO}_2 + \text{RONO}_{2(\text{g+p})} + \text{NO}_3^-_{(\text{g+p})}$. Mixing ratios of each species are determined as the difference between adjacent channels, i.e., $\text{NO}_3^-_{(\text{g+p})}$ equals the 600°C channel minus the signal in the 400°C channel. ClNO_2 is thought to appear primarily in the 400°C channel. Recent observations indicated that about 50 % of ClNO_2 was observed in the 400°C channel and 50 % in the 600°C channel. Residence times in the ovens are sufficient to volatilize aerosol-bound nitrates, which is reflected in the $\text{RONO}_{2(\text{g+p})} + \text{NO}_3^-_{(\text{g+p})}$ subscripting (Day et al., 2002).

$\text{NO}_3^-_{(\text{p})}$ was measured onboard the P-3B by a PILS system sampling at 4 min time resolution with a well-characterized $\sim 3\ \mu\text{m}$ aerosol size cutoff. In Fig. A1, 4 min averaged $\text{NO}_3^-_{(\text{g+p})}$ measured by TD-LIF is compared against PILS $\text{NO}_3^-_{(\text{p})}$ when the aircraft was below 0.5 km a.s.l. The data are fit using a linear least squares model that assumes equally weighted errors in both measurements. Reported uncertainties in the TD-LIF and PILS observations are 15 and 20 %, respectively, and they correlate ($y = 0.8x + 2.3$) within combined uncertainties of 25 %. The TD-LIF is sensitive to $\text{HNO}_{3(\text{g})}$, while the PILS is not. Using ISORROPIA II (described in Sect. 4.2) $\text{HNO}_{3(\text{g})}$ is predicted to be up to a few ppb in the afternoon, corresponding to the highest temperatures but not to the highest $\text{NO}_3^-_{(\text{p})}$ (Fig. 7). Additional details on the TD-LIF aircraft inlet configuration are found in Perring et al. (2009) and Wooldridge et al. (2010).

A3 Data and filtering for boundary layer sampling

Occasionally the height of the daytime boundary layer was observed near the altitude of the P-3B's low-level flight legs, requiring analysis to distinguish between free troposphere and boundary layer air. Within boundary layer sampling was identified using $1\ \text{s}^{-1}$ measurements of NO and RH recorded by the aircraft data system, according to steep discontinuities in both tracers, being high in the boundary layer and low aloft. In some cases, $\text{H}_2\text{O}_{(\text{v})}$ measured by diode laser hygrometer and O_3 were also considered. In Fig. 3 in addition to filtering for within boundary layer sampling, data were only plotted when the pressure altitude (a.s.l.) was greater than 0.

For our derivation of $\tau_{\text{NO}_3^-}$, boundary layer depth was estimated with data from an MPL located in the town of Porterville during DISCOVER-AQ. The MPL was supplemented with a wide-field receiver system that allowed for improved near-range signal recovery of the 527 nm attenuated backscatter profiles that were recorded at 30 m vertical and 1 min time resolutions. For daytime mixed-layer conditions driven by convection, the aerosol gradient falls off and stable molecular scatter signal above the lowest mixed aerosol layer signal represents the boundary layer height. According to this aerosol gradient, boundary layer heights were observed to range from 300 to 700 m during DISCOVER-AQ.

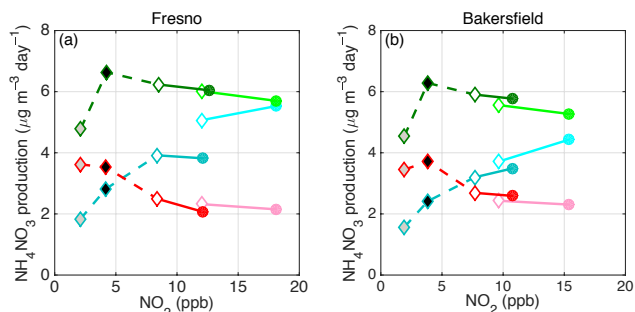


Figure B1. Wintertime NH_4NO_3^- production ($\mu\text{g m}^{-3} \text{ day}^{-1}$) by OH-initiated chemistry versus daytime (10:00–15:00 LT) NO_2 (ppb) for each individual HO_x precursor: $\text{O}(^1\text{D}) + \text{H}_2\text{O}$ (red), HONO (turquoise), and CH_2O (green). Data are tethered present-day 3-year medians on weekdays (closed circles) and weekends (open diamonds) in Fresno (a) and Bakersfield (b). Lighter tint data are tethered 3-year medians at the start of the record (2001–2004). There is no significant difference between medians and means. Predicted NH_4NO_3^- production calculated at -50% weekend NO_x (NO_x black-filled diamond) and -75% weekend NO_x (gray-filled diamond) are also shown.

Appendix B: Calculating PNO_3^-

The chemistry producing NO_3 radical at night and HNO_3 in the daytime is shown in Fig. B1 as a function of NO_2 . The production of NO_3 radical ($\mu\text{g m}^{-3} \text{ h}^{-1}$) is calculated at four initial O_x ($\text{O}_x \equiv \text{NO}_2 + \text{O}_3$) conditions: 50 ppb O_x (black), 40 ppb O_x (purple), 30 ppb O_x (violet), and 20 ppb O_x (gray). In Fig. B1b, the production of HNO_3 is shown for two PHO_x conditions: $0.3 \text{ ppt s}^{-1} \text{ PHO}_x$ (orange) and $0.15 \text{ ppt s}^{-1} \text{ PHO}_x$ (golden). For the sake of the night–day comparison, in Fig. B1 NO_3 radical production is scaled by two, which assumes all NO_3 reacts with NO_2 and that N_2O_5 hydrolysis is rapid compared to $\text{NO}_2 + \text{O}_3$. In this analysis, we compute PNO_3^- as NO_3 radical production scaled by the observationally constrained NO_3 radical reactivity yielding NO_3^- (see text below).

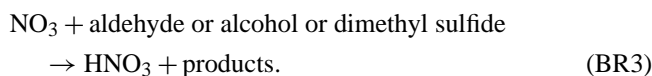
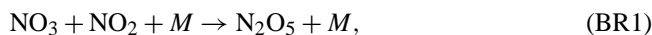
B1 NO_3 -initiated PNO_3^- in the nocturnal residual layer

Our time-dependent box model of NO_3 radical production was run separately for each day over the time period 2000–2013. The model was initialized with hourly O_3 measurements at the surface using the maximum O_3 concentration 1–3 h before sunset and the median daytime (10:00–15:00 LT) NO_x . This window was determined based on the timing of steep afternoon O_3 titration observed in the hourly surface O_3 data, both during DISCOVER-AQ and throughout the interannual record. O_3 and NO_x were treated as well mixed in the daytime boundary layer and $k_{\text{NO}_2+\text{O}_3}$ was calculated based on the mean surface temperature at 18:00–20:00 LT. NO_3 radical production was integrated from sunset to 1 h

prior to sunrise. Differences were insignificant using mean O_3 over this time window versus the daily maximum.

Although there is no long-term, vertically resolved measurement record of any species in the region, there is observational evidence that the rapid decline in afternoon O_3 corresponds to the stratification of the daytime boundary layer. First, as part of CRPAQS, measurements of NO , O_3 , and NO_3^- were made simultaneously atop a tower (90 m a.g.l.) and at a lower level (7 m a.g.l.) in the SJV town of Angiola. Winter average (December 2000–January 2001) NO and O_3 at the two sampling heights were comparable from 10:00 to 13:00 LT; however, by 14:00 LT the concentrations began to diverge, with O_3 at 7 m falling rapidly ($\sim 5 \text{ ppb h}^{-1}$), concurrent with increases in NO , while O_3 at 90 m remaining approximately constant until sunset, whereupon a decrease of $\sim 2 \text{ ppb h}^{-1}$ was observed. NO at the 90 m level was near 0 throughout the night. A 7-day time series of NO_3^- data at 90 m showed clear increases in NO_3^- beginning at nightfall and persisting until sunrise of $\sim 10 \mu\text{g m}^{-3}$ (Brown et al., 2006). These diurnal patterns suggest that the NRL(s) decouple from the surface layer ~ 3 h prior to sunset and that initial concentrations of the nocturnal chemistry reactants, NO_2 and O_3 , are also represented by surface concentrations 3 h prior to sunset. During DISCOVER-AQ, full vertical profiling by the P-3B (including a missed approach) concluded in Fresno at 14:30–15:30, ~ 2 – 3 h prior to sunset. Profiles of O_3 and the conserved tracer O_x suggest that stratification of the daytime boundary layer had begun by this time on multiple afternoons, although day-to-day variability was observed. A comparison of mean O_3 and O_x concentrations in the top 100 m (~ 0.35 – 0.45 km a.s.l.) and bottom 100 m (~ 0.15 – 0.05 km a.s.l.) of the atmosphere below the height of the daytime boundary layer, found small differences in O_x on all flight days but, on some days, large differences in O_3 . O_3 variations equaled 25–30% the mean O_3 profile concentration on two days, 18 and 22 January 2013. At midday (12:00–13:00) at the same altitudes, small absolute differences were observed in both O_3 and O_x .

Reaction fates of the NO_3 radicals calculated by the time-dependent box model described above were determined according to the mean proportional NO_3 reactivity contributions observed during DISCOVER-AQ. NO_3 Reactions (BR3–BR5) are as follows:



Each of the three pathways results in a different number of NO_3^- produced per NO_3 radical. NO_3 reactivities are defined as $k_{\text{N}_2\text{O}_5} \text{K}_{\text{eq}}(T) [\text{NO}_2]$ (Brown

et al., 2003, 2009), $\sum_i k_{\text{NO}_3+\text{alkene}_i} [\text{alkene}_i]$, and $\sum_i (k_{\text{NO}_3+\text{alcohol}_i} [\text{alcohol}_i] + k_{\text{NO}_3+\text{aldehyde}_i} [\text{aldehyde}_i] + k_{\text{NO}_3+\text{DMS}} [\text{DMS}])$, for Reactions (BR3), (BR4), and (BR5), respectively. $k_{\text{N}_2\text{O}_5=0.25\bar{v}A\gamma} (\text{N}_2\text{O}_5)$ is the N₂O₅ uptake coefficient and $K_{\text{eq}}(T)$ is Reaction (R3) equilibrium constant. For $k_{\text{N}_2\text{O}_5}$, \bar{v} is the N₂O₅ mean molecular speed, A is the aerosol surface area density, and γ (N₂O₅) is the N₂O₅ aerosol uptake coefficient. A was determined as the product of the dry surface area of particles 60–1000 nm in diameter measured by an ultra-high sensitivity aerosol spectrometer and the hygroscopic growth factor, $f(\text{RH})$, calculated from the signal difference of a two nephelometers, one sampling dried air (RH < 40 %) and a second sampling after humidification to 80 % RH (each measurement was made onboard the P-3B). During DISCOVER-AQ, below 0.4 km a.s.l., the mean dry surface area was $191.8 \pm 75 \mu\text{m}^2 \text{cm}^{-3}$ (1 σ) and the mean $f(\text{RH})$ was 1.7 ± 0.2 (1 σ). γ (N₂O₅) was set equal to 0.006 as estimated from the parameterization in Bertram and Thornton (2009) following Wagner et al. (2013): 30 M aerosol water and an aerosol system including only water, NH₄⁺, and NO₃⁻. Using the aerosol water, NH₄⁺, and NO₃⁻ that we computed by ISORROPIA II, NO₃⁻ constituted 45 % aerosol mass. We assume that all N₂O₅ was converted to 2NO₃⁻. If ClNO₂ formation is an important N₂O₅ hydrolysis product in the SJV, we have overestimated the total NO₃⁻ production. While there is limited observational insight into the extent of ClNO₂ formation, because ClNO₂ is predicted to thermally dissociate in the RONO₂ channel of the TD-LIF instrument (reviewed in Perring et al., 2013), in the early morning, a portion of the measured quantity RONO_{2(g+p)} is possibly due to ClNO₂. On all days, the P-3B flights began at ~08:00 LT, which is early enough to capture at least portion of nocturnal ClNO₂ prior to photolysis. The mean RONO_{2(g+p)} before 10:00 and below 0.4 m a.s.l is equivalent to $1.6 \mu\text{g m}^{-3}$ NO₃⁻, or 15 % of measured NO₃⁻_(g+p). However, there is little discernable loss of RONO_{2(g+p)} in the late morning, which would be expected if the RONO_{2(g+p)} was due to ClNO₂, suggesting 15 % is an upper limit.

NO₃ reactivities were computed using the DISCOVER-AQ data set with daytime (13:00–17:00 LT) surface observations of NO₂, organic compounds (whole air canister sampling), and dimethyl sulfide (DMS) (whole air canister sampling). CH₂O measurements from onboard the P3-B were included in the speciated reactivity for Reaction (BR5). Little temporal variability was observed in the concentrations of organic compounds between 13:00 and 17:00 LT. If alkenes reactive with NO₃ in NRL are oxidized by OH or O₃ prior to nightfall, then $\sum_i k_{\text{NO}_3+\text{alkene}_i} [\text{alkene}_i]$ represents an overestimate. This will alter the absolute value of the calculated change in $P\text{NO}_3^-$ but not the functional form of the dependence. To account for this, we decrease the concentrations

of organic species by one e-fold prior to computing the NO₃ reactivity.

In Fresno and Bakersfield the reaction of NO₂ with NO₃ represented ~80 % of total NO₃ reactivity, with negligible weekday–weekend differences. The mean NO₃ reactivity values used in the model were 0.005 s^{-1} for addition to double bonds, yielding 0 HNO₃; $<0.001 \text{ s}^{-1}$ for hydrogen abstraction, yielding 1 HNO₃; and 0.02 s^{-1} for reaction with NO₂, which after heterogeneous conversion of N₂O₅ yields 2 HNO₃. This gives 1.5 NO₃⁻ produced per NO₃ on average. The integrated $P\text{NO}_3^-$ was taken as the NO₃ radical production scaled by the NO₃ reactivity to NO₂, which assumed reactions with alkenes and DMS were instantaneous. This result is similar to that of the wintertime NACHTT experiment at comparable relative NO₂ concentrations (Wagner et al., 2013). During NACHTT NO₃ and N₂O₅ were measured, the kinetics of N₂O₅ explicitly included in the calculation of $P\text{NO}_3^-$, and 1.6 HNO₃ per NO₃ radical produced was inferred.

B2 NO₃-initiated $P\text{NO}_3^-$ in the nocturnal boundary layer

The production of NO₃ radical was directly computed from surface measurements of hourly O₃, NO₂, NO, and temperature each day from 2000 to 2013. NO₃ production was integrated between sunset and 1 h prior to sunrise and scaled by 1.1 NO₃⁻ produced per NO₃, which is the result from the NO₃ reactivity calculation described above with no organic reactivity loss. There were times that under conditions of very high NO that nighttime O₃ was observed to be positive and constant at nonphysical values of 1–10 ppb for multiple hours. This offset was interpreted as a measurement artifact as excess NO titrates O₃ completely. To account for this, when NO_x was greater than 5 times the reported O₃, O₃ was set equal to 0 prior to computing NO₃ production. However, concentrations of DMS and organic emissions, largely anthropogenic in origin in the wintertime SJV, are predicted to be higher in the NBL than in the daytime boundary layer.

B3 OH-initiated $P\text{NO}_3^-$

The integrated daily production of HNO₃ was calculated for each day from 2000 to 2013 separately for each of the three HO_x sources: O(¹D) + H₂O, HONO photolysis, and CH₂O photolysis (Eq. B1). $P\text{NO}_3^-$ versus NO₂ attributed to each HO_x source is plotted in Fig. B2. OH was modeled with an analytical model constrained to DISCOVER-AQ observations, built on the assumption that oxidizing radicals were in steady state (Eq. B2) and that RO₂ and HO₂ production are approximately equal, as are RO₂ production and loss, giving Eq. (B3) for both RO₂ and HO₂ (Murphy et al., 2007). The symbol α is the RONO₂ branching ratio. RO₂NO₂ are considered to be in thermal equilibrium with NO₂ and peroxy radicals and therefore not to contribute to

net radical formation. Calculated wintertime OH values were $\sim 10^6$ molecules cm^{-3} at noontime and exhibited reasonable nonlinear NO₂ dependence throughout the day. Observational inputs to the model were NO and NO₂, the total organic reactivity to OH (VOCR), PHO_x , α , and temperature. VOCR was computed as equal to $\sum_i k_{OH+VOC_i}[VOC_i]$ using whole air samples of speciated organic molecules collected at the ground during DISCOVER-AQ and CH₂O data from onboard the P-3B, as VOCR equal to $\sum_i k_{OH+VOC_i}[VOC_i]$. The daytime average was $\sim 4 \text{ s}^{-1}$, consistent with a recent analysis of the temperature dependence of total VOCR in Bakersfield (Pusede et al., 2014), giving confidence that the majority of the reactivity was accounted for. The α is set equal to 2%. Equations (B2) and (B3) are combined to solve for OH.

$$PHO_x = 2j_{O_3 \rightarrow O^1D}[O_3] \frac{k[H_2O]}{k[H_2O] + k[N_2 + O_2]} + 2j_{CH_2O}[CH_2O] + j_{HONO}[HONO] \quad (B1)$$

$$PHO_x = LHO_x = 2k_{HO_2+HO_2}[HO_2]^2 + 2k_{HO_2+RO_2}[HO_2][RO_2] + 2k_{RO_2+RO_2}[RO_2]^2 + k_{NO_2+OH}[NO_2][OH] + \alpha k_{NO+RO_2}[NO][RO_2] \quad (B2)$$

$$[RO_2] \sim [HO_2] = \frac{VOCR[OH]}{(1 - \alpha)k_{NO+RO_2}[NO]} \quad (B3)$$

Noontime j_{O_3} , j_{HONO} , and j_{CH_2O} were computed with the TUV calculator, http://cprm.acd.ucar.edu/Models/TUV/Interactive_TUV (Madronich, 1987), on a clear-sky day (20 January, 2013), scaled by the ratio of the TUV j_{NO_2} and a measurement of j_{NO_2} made onboard the P-3B, and combined with the diurnally varying long-term record of solar radiation.

The trend in $O(^1D) + H_2O$ was calculated from the observational record of O₃, RH, and solar radiation.

No multi-year measurements of HONO have been reported in US cities. HONO is formed at night by a mechanism functionally equivalent to the conversion of two NO₂ to one gas-phase HONO and one ground-surface adsorbed HNO₃ molecule (Finlayson-Pitts et al., 2003). We computed HONO as equal to 4% the nighttime (10:00–18:00 LT) mean NO₂ (Stutz et al., 2004), yielding one HONO data point for each day. This HONO initialized a calculation wherein photolytic loss was computed, giving HONO concentrations at 1 h time resolution. We have not accounted for daytime formation; however, in total, daytime source(s) are weekday-weekend independent (Pusede et al., 2015).

The interannual trend in CH₂O is also unconstrained with observations. In the winter, CH₂O is not monitored at the surface and cannot be quantified from space due to low column concentrations and shallow daytime boundary layers. CH₂O is a primary organic emission from agricultural activities associated with animal feeds (Howard et al., 2010), dairy cows (Shaw et al., 2007), and combustion. State inventories offer little insight into CH₂O trends, as it is unknown whether a priori accounts are complete. CH₂O is also the oxidation product of most organic molecules in the atmosphere. We calculated the CH₂O concentration using a 0-D chemical model constrained to the complete 1 min DISCOVER-AQ data set. All 95 organic molecules measured by whole air sampling at the ground level at the Fresno site were included after scaling by a fit to aircraft carbon monoxide. Within the boundary layer, modeled CH₂O typically captured 75% of the CH₂O measured on the P-3B, with the discrepancy most likely due to the local primary CH₂O emissions. We ran the model under four NO_x reduction scenarios, –75% NO_x, –50% NO_x, +50% NO_x, and +75% NO_x assuming the portion of CH₂O not captured by our model remained constant. At 50% higher NO_x, i.e., at the start of the record, secondary CH₂O was $\sim 10\%$ lower on weekdays and $\sim 5\%$ lower on weekends than in the base model (2013 conditions). At –50% and –75% NO_x, in the next decade, secondary CH₂O is predicted to increase by 15–25% from 2013 week-end NO_x levels, as reductions in NO_x increase OH.

The integrated wintertime 24 h NH₄NO₃ production for each of the three HO_x sources is shown in Fig. B2, along with the projected response of to changes in NO_x of –50% and –75% from weekend concentrations. PNO_3^- attributed to $O(^1D) + H_2O$ is $2\text{--}3 \mu\text{g m}^{-3} \text{ day}^{-1}$ (2000–2013) and has increased by $\sim 0.1 \mu\text{g m}^{-3} \text{ ppb}^{-1} \text{ NO}_2$ in all three SJV cities. It is an order of magnitude smaller than PNO_3^- in the NRL in the wintertime average. NH₄NO₃ production attributed to HONO has decreased with reduced NO₂, i.e., the trend has the correct sign compared to NO₃[–] concentrations (Fig. 2). Declines in HONO have resulted in a decrease in NH₄NO₃ production of $3\text{--}6 \mu\text{g m}^{-3} \text{ day}^{-1}$ over the entire NO₂ range. We find that CH₂O, observed to be 2.3 ± 1.1 ppb (1σ) in Fresno and 2.0 ± 0.9 ppb in Bakersfield, has been the largest contributor to photochemical production of NH₄NO₃ at $\sim 6 \mu\text{g m}^{-3} \text{ day}^{-1} \text{ NO}_3^-$.

Appendix C: Additional details regarding $\tau_{\text{NO}_3^-}$

The timing of decoupling between the NBL and the NRL(s) has implications for our derivation of $\tau_{\text{NO}_3^-}$. Observed daily $\frac{\partial \text{NO}_3^-}{\partial t}$ are consistent with the majority of NO_3^- lost via deposition of $\text{HNO}_{3(\text{g})}$ from most of the daytime boundary layer. If loss occurred from only the lowest 50 m of the daytime boundary layer, then the observationally derived $\text{HNO}_{3(\text{g})} v_d$ would be only 0.4 cm s^{-1} , below direct measurements (e.g., Huebert and Robert, 1985; Meyers et al., 1989; Sievering et al., 2001; Volpe Horii et al., 2005; Farmer et al., 2006). Gaseous HNO_3 that does not deposit will repartition to the aerosol phase when temperatures fall and RH rises in the evening. Assuming an NBL height of 50–100 m, then a nighttime rise (black data in Fig. 7) of 10–5 fold is expected. An NO_3^- concentration of $10 \mu\text{g m}^{-3}$ shifted to the gas phase would increase by $100\text{--}50 \mu\text{g m}^{-3}$ at nightfall. By contrast, typical nighttime increases were $0\text{--}15 \mu\text{g m}^{-3}$.

In Fig. C1 we show low-altitude (20–350 m a.g.l.) observations from the P-3B colored by $\text{NO}_3^-_{(\text{g+p})}$ concentration over the city of Visalia on 5 flight days as evidence that afternoon decreases are net $\text{HNO}_3 + \text{NO}_3^-$ loss and not a shift in partitioning between the two species. In each panel the left-hand flight track was at midday (12:00–13:00 LT) and the right-hand track, shifted in space by 0.02° longitude for visual clarity, was in afternoon (15:00–16:00 LT). On each of the five flights, ~ 2 -fold higher concentrations of $\text{NO}_3^-_{(\text{g+p})}$ were observed at midday compared to a few hours later. Additionally, the reduction in $\text{NO}_3^-_{(\text{g+p})}$ is apparent at the higher altitudes, shown in the top and bottom third of each panel, suggesting the loss in NO_3^- measured by AMS at the surface in Fresno does extend up to at least 300–350 m a.g.l.

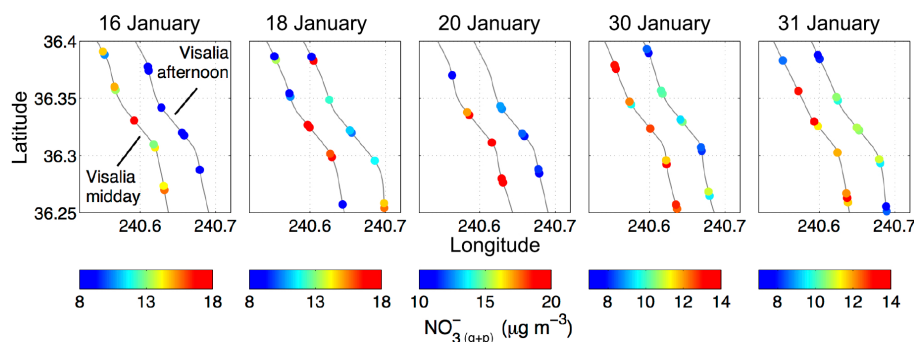


Figure C1. $\text{NO}_3^-_{(\text{g+p})}$ ($\mu\text{g m}^{-3}$) in $\text{PM}_{2.5}$ measured during 10 missed approaches on 5 days over Visalia. The left-hand flight track is the midday (12:00–13:00 LT) missed approach and the right-hand track, shifted east by 0.02° , is the afternoon (15:00–16:00 LT) missed approach.

Acknowledgements. This work was funded by NASA under grant NNX10AR36G. Q. Zhang and C. D. Cappa were also supported by the California Air Resources Board (contract no. 14-307). We acknowledge use of publicly available data maintained by the US EPA, California Air Resources Board, and California Irrigation Management Information System. We thank John Barrick for the j_{NO_2} and RH (PDS) data, Glenn Diskin for the H₂O_(v) (DLH) data, Luke Ziemba and Lee Thornhill for the $f(\text{RH})$ and UHSAS data, and Donald Blake for the speciated organic compound data. We thank Melinda Beaver for assistance interpreting the long-term ozone data. We thank Steve S. Brown for his feedback during the review process. This analysis would not have been possible without the work of the pilots, crew, and engineers of the NASA P-3B.

Edited by: N. M. Donahue

References

- American Lung Association, State of the air: 2014 report: <http://www.stateoftheair.org/2014/assets/ALA-SOTA-2014-Full.pdf> (last access: 27 March 2015), 2014.
- Appel, B. R., Tokiwa, Y., and Haik, M.: Sampling of nitrates in ambient air, *Atmos. Environ.*, 15, 283–289, doi:10.1016/0004-6981(81)90029-9, 1981.
- Babich, P., Davey, M., Allen, G., and Koutrakis, P.: Method comparisons for particulate nitrate, elemental carbon, and PM_{2.5} mass in seven U.S. cities, *J. Air Waste Ma.*, 50, 1095–1105, doi:10.1080/10473289.2000.10464152, 2000.
- Bao, J. W., Michelson, S. A., Persson, P. O. G., Djalalova, I. V., and Wilczak, J. M.: Observed and WRF-Simulated Low-Level Winds in a High-Ozone Episode during the Central California Ozone Study, *J. Appl. Meteorol. Clim.*, 47, 2372–2394, doi:10.1175/2008JAMC1822.1, 2008.
- Bertram, T. H. and Thornton, J. A.: Toward a general parameterization of N₂O₅ reactivity on aqueous particles: the competing effects of particle liquid water, nitrate and chloride, *Atmos. Chem. Phys.*, 9, 8351–8363, doi:10.5194/acp-9-8351-2009, 2009.
- Bianco, L., Djalalova, I. V., King, C. W., and Wilczak, J. M.: Diurnal evolution and annual variability of boundary-layer height and its correlation to other meteorological variables in California's Central Valley, *Bound.-Lay. Meteorol.*, 140, 491–511, doi:10.1007/s10546-011-9622-4, 2011.
- Brown, S. S. and Stutz, J.: Nighttime radical observations and chemistry, *Chem. Soc. Rev.*, 41, 6405–6447, doi:10.1039/C2CS35181A, 2012.
- Brown, S. G., Hyslop, N. P., Roberts, P. T., McCarthy, M. C., and Lurmann, F. W.: Wintertime vertical variations in particulate matter (PM) and precursor concentrations in the San Joaquin Valley during the California Regional Coarse PM/Fine PM Air Quality Study, *J. Air Waste Ma.*, 56, 1267–1277, doi:10.1080/10473289.2006.10464583, 2006.
- Brown, S. S., Stark, H., and Ravishankara, A. R.: Applicability of the steady state approximation to the interpretation of atmospheric observations of NO₃ and N₂O₅, *J. Geophys. Res.*, 108, 4539, doi:10.1029/2003JD003407, 2003.
- Brown, S. S., Dubé, W. P., Osthoff, H. D., Wolfe, D. E., Angevine, W. M., and Ravishankara, A. R.: High resolution vertical distributions of NO₃ and N₂O₅ through the nocturnal boundary layer, *Atmos. Chem. Phys.*, 7, 139–149, doi:10.5194/acp-7-139-2007, 2007.
- Brown, S. S., Dube, W. P., Fuchs, H., Ryerson, T. B., Wollny, A. G., Brock, C. A., Bahreini, R., Middlebrook, A. M., Neuman, J. A., Atlas, E., Roberts, J. M., Osthoff, H. D., Trainer, M., Fehsenfeld, F. C., and Ravishankara, A. R.: Reactive uptake coefficients for N₂O₅ determined from aircraft measurements during the Second Texas Air Quality Study: comparison to current model parameterizations, *J. Geophys. Res.-Atmos.*, 114, D00F10, doi:10.1029/2008jd011679, 2009.
- California Air Resources Board, Truck and bus regulation—current regulation and advisories, <http://www.arb.ca.gov/msprog/onrdiesel/regulation.htm> (last access: 7 January 2016), 2012.
- Chan, A. W. H., Chan, M. N., Surratt, J. D., Chhabra, P. S., Loza, C. L., Crouse, J. D., Yee, L. D., Flagan, R. C., Wennberg, P. O., and Seinfeld, J. H.: Role of aldehyde chemistry and NO_x concentrations in secondary organic aerosol formation, *Atmos. Chem. Phys.*, 10, 7169–7188, doi:10.5194/acp-10-7169-2010, 2010.
- Chen, L. W. A., Watson, J. G., Chow, J. C., and Magliano, K. L.: Quantifying PM_{2.5} source contributions for the San Joaquin Valley with multivariate receptor models, *Environ. Sci. Technol.*, 41, 2818–2826, doi:10.1021/es0525105, 2007.
- Chow, J., Watson, J., Lowenthal, D., Park, K., Doraiswamy, P., Bowers, K., and Bode, R.: Continuous and filter-based measurements of PM_{2.5} nitrate and sulfate at the Fresno Supersite, *Environ. Monit. Assess.*, 144, 179–189, doi:10.1007/s10661-007-9987-5, 2008.
- Chow, J. C., Watson, J. G., Lowenthal, D. H., and Magliano, K. L.: Loss of PM_{2.5} nitrate from filter samples in Central California, *J. Air Waste Ma.*, 55, 1158–1168, doi:10.1080/10473289.2005.10464704, 2005.
- Chow, J. C., Chen, L. W. A., Watson, J. G., Lowenthal, D. H., Magliano, K. A., Turkiewicz, K., and Lehrman, D. E.: PM_{2.5} chemical composition and spatiotemporal variability during the California Regional PM₁₀/PM_{2.5} Air Quality Study (CRPAQS), *J. Geophys. Res.-Atmos.*, 111, D10S04, doi:10.1029/2005jd006457, 2006.
- Clarise, L., Shephard, M. W., Dentener, F., Hurtmans, D., Cady-Pereira, K., Karagulian, F., Van Damme, M., Clerbaux, C., and Coheur, P.-F.: Satellite monitoring of ammonia: a case study of the San Joaquin Valley, *J. Geophys. Res.-Atmos.*, 115, D13302, doi:10.1029/2009jd013291, 2010.
- Cosman, L. M. and Bertram, A. K.: Reactive uptake of N₂O₅ on aqueous H₂SO₄ solutions coated with 1-component and 2-component monolayers, *J. Phys. Chem. A*, 112, 4625–4635, doi:10.1021/jp8005469, 2008.
- Dallmann, T. R. and Harley, R. A.: Evaluation of mobile source emission trends in the United States, *J. Geophys. Res.-Atmos.*, 115, D14305, doi:10.1029/2010jd013862, 2010.
- Dallmann, T. R., DeMartini, S. J., Kirchstetter, T. W., Herndon, S. C., Onasch, T. B., Wood, E. C., and Harley, R. A.: On-road measurement of gas and particle phase pollutant emission factors for individual heavy-duty diesel trucks, *Environ. Sci. Technol.*, 46, 8511–8518, doi:10.1021/es301936c, 2012.
- Day, D. A., Wooldridge, P. J., Dillon, M. B., Thornton, J. A., and Cohen, R. C.: A thermal dissociation laser-induced fluorescence instrument for in situ detection of NO₂, peroxy nitrates, alkyl nitrates, and HNO₃, *J. Geophys. Res.-Atmos.*, 107, 4046, doi:10.1029/2001JD000779, 2002.

- Dentener, F. J. and Crutzen, P. J.: Reaction of N₂O₅ on tropospheric aerosols – impact on the global distributions of NO_x, O₃, and OH, *J. Geophys. Res.-Atmos.*, 98, 7149–7163, doi:10.1029/92jd02979, 1993.
- Drewnick, F., Hings, S. S., DeCarlo, P., Jayne, J. T., Gonin, M., Fuhrer, K., Weimer, S., Jimenez, J. L., Demerjian, K. L., Borrmann, S., and Worsnop, D. R.: A new Time-of-Flight Aerosol Mass Spectrometer (TOF-AMS) – instrument description and first field deployment, *Aerosol Sci. Technol.*, 39, 637–658, doi:10.1080/02786820500182040, 2005.
- Dunlea, E. J., Herndon, S. C., Nelson, D. D., Volkamer, R. M., San Martini, F., Sheehy, P. M., Zahniser, M. S., Shorter, J. H., Wormhoudt, J. C., Lamb, B. K., Allwine, E. J., Gaffney, J. S., Marley, N. A., Grutter, M., Marquez, C., Blanco, S., Cardenas, B., Retama, A., Ramos Villegas, C. R., Kolb, C. E., Molina, L. T., and Molina, M. J.: Evaluation of nitrogen dioxide chemiluminescence monitors in a polluted urban environment, *Atmos. Chem. Phys.*, 7, 2691–2704, doi:10.5194/acp-7-2691-2007, 2007.
- Environmental Protection Agency, California's advanced clean cars program: http://www.arb.ca.gov/msprog/clean_cars/accsummary-final.pdf (last access: 7 January 2016), 2012.
- Environmental Protection Agency, EPA revises the National Ambient Air Quality Standards for particle pollution: <https://www.gpo.gov/fdsys/pkg/FR-2013-01-15/pdf/2012-30946.pdf> (last access: 7 January 2016), 2013.
- Farmer, D. K., Wooldridge, P. J., and Cohen, R. C.: Application of thermal-dissociation laser induced fluorescence (TD-LIF) to measurement of HNO₃, alkyl nitrates, peroxy nitrates, and NO₂ fluxes using eddy covariance, *Atmos. Chem. Phys.*, 6, 3471–3486, doi:10.5194/acp-6-3471-2006, 2006.
- Farmer, D. K., Chen, Q., Kimmel, J. R., Docherty, K. S., Nemitz, E., Artaxo, P. A., Cappa, C. D., Martin, S. T., and Jimenez, J. L.: Chemically resolved particle fluxes over tropical and temperate forests, *Aerosol Sci. Technol.*, 47, 818–830, doi:10.1080/02786826.2013.791022, 2013.
- Finlayson-Pitts, B. J., Wingen, L. M., Sumner, A. L., Syomin, D., and Ramazan, K. A.: The heterogeneous hydrolysis of NO₂ in laboratory systems and in outdoor and indoor atmospheres: An integrated mechanism, *Phys. Chem. Chem. Phys.*, 5, 223–242, doi:10.1039/b208564j, 2003.
- Flechar, C. R., Spirig, C., Neftel, A., and Ammann, C.: The annual ammonia budget of fertilised cut grassland – Part 2: Seasonal variations and compensation point modeling, *Biogeosciences*, 7, 537–556, doi:10.5194/bg-7-537-2010, 2010.
- Fountoukis, C. and Nenes, A.: ISORROPIA II: a computationally efficient thermodynamic equilibrium model for K⁺-Ca²⁺-Mg²⁺-NH₄⁺-Na⁺-SO₄²⁻-NO₃⁻-Cl⁻-H₂O aerosols, *Atmos. Chem. Phys.*, 7, 4639–4659, doi:10.5194/acp-7-4639-2007, 2007.
- Fry, J. L., Draper, D. C., Zarzana, K. J., Campuzano-Jost, P., Day, D. A., Jimenez, J. L., Brown, S. S., Cohen, R. C., Kaser, L., Hansel, A., Cappellin, L., Karl, T., Hodzic Roux, A., Turnipseed, A., Cantrell, C., Lefer, B. L., and Grossberg, N.: Observations of gas- and aerosol-phase organic nitrates at BEACHON-RoMBAS 2011, *Atmos. Chem. Phys.*, 13, 8585–8605, doi:10.5194/acp-13-8585-2013, 2013.
- Ge, X., Setyan, A., Sun, Y., and Zhang, Q.: Primary and secondary organic aerosols in Fresno, California during wintertime: results from high resolution aerosol mass spectrometry, *J. Geophys. Res.-Atmos.*, 117, D19301, doi:10.1029/2012JD018026, 2012.
- Gilliland, A. B., Appel, K. W., Pinder, R. W., and Dennis, R. L.: Seasonal NH₃ emissions for the continental United States: inverse model estimation and evaluation, *Atmos. Environ.*, 40, 4986–4998, doi:10.1016/j.atmosenv.2005.12.066, 2006.
- Goebes, M. D., Strader, R., and Davidson, C.: An ammonia emission inventory for fertilizer application in the United States, *Atmos. Environ.*, 37, 2539–2550, doi:10.1016/s1352-2310(03)00129-8, 2003.
- Hallquist, M., Stewart, D. J., Stephenson, S. K., and Cox, R. A.: Hydrolysis of N₂O₅ on sub-micron sulfate aerosols, *Phys. Chem. Chem. Phys.*, 5, 3453–3463, doi:10.1039/b301827j, 2003.
- Heald, C. L., Collett Jr., J. L., Lee, T., Benedict, K. B., Schwandner, F. M., Li, Y., Clarisse, L., Hurtmans, D. R., Van Damme, M., Clerbaux, C., Coheur, P.-F., Philip, S., Martin, R. V., and Pye, H. O. T.: Atmospheric ammonia and particulate inorganic nitrogen over the United States, *Atmos. Chem. Phys.*, 12, 10295–10312, doi:10.5194/acp-12-10295-2012, 2012.
- Hering, S. and Cass, G.: The magnitude of bias in the measurement of PM_{2.5} arising from volatilization of particulate nitrate from teflon filters, *J. Air Waste Ma.*, 49, 725–733, doi:10.1080/10473289.1999.10463843, 1999.
- Herner, J. D., Ying, Q., Aw, J., Gao, O., Chang, D. P. Y., and Kleeman, M. J.: Dominant mechanisms that shape the airborne particle size and composition distribution in Central California, *Aerosol Sci. Technol.*, 40, 827–844, doi:10.1080/02786820600728668, 2006.
- Holets, S. and Swanson, R. N.: High-inversion fog episodes in Central California, *J. Appl. Meteorol.*, 20, 890–899, doi:10.1175/1520-0450(1981)020<0890:HIFEIC>2.0.CO;2, 1981.
- Howard, C. J., Kumar, A., Malkina, I., Mitloehner, F., Green, P. G., Flocchini, R. G., and Kleeman, M. J.: Reactive organic gas emissions from livestock feed contribute significantly to ozone production in Central California, *Environ. Sci. Technol.*, 44, 2309–2314, doi:10.1021/es902864u, 2010.
- Hu, J. H. and Abbatt, J. P. D.: Reaction probabilities for N₂O₅ hydrolysis on sulfuric acid and ammonium sulfate aerosols at room temperature, *J. Phys. Chem. A*, 105, 871–878, doi:10.1021/jp9627436, 1997.
- Huebert, B. J. and Robert, C. H.: The dry deposition of nitric acid to grass, *J. Geophys. Res.-Atmos.*, 90, 2085–2090, doi:10.1029/JD090iD01p02085, 1985.
- Jacob, D. J., Waldman, J. M., Munger, J. W., and Hoffmann, M. R.: A field investigation of physical and chemical mechanisms affecting pollutant concentrations in fog droplets, *Tellus*, 36, 272–285, doi:10.1111/j.1600-0889.1984.tb00247.x, 1984.
- Jacob, D. J., Munger, J. W., Waldman, J. M., and Hoffmann, M. R.: The H₂SO₄-HNO₃-NH₃ system at high humidities and in fogs. 1. Spatial and temporal patterns in the San Joaquin Valley of California, *J. Geophys. Res.-Atmos.*, 91, 1073–1088, doi:10.1029/JD091iD01p01073, 1986a.
- Jacob, D. J., Waldman, J. M., Munger, J. W., and Hoffmann, M. R.: The H₂SO₄-HNO₃-NH₃ system at high humidities and in fogs. 2. Comparison of field data with thermodynamic calculations, *J. Geophys. Res.-Atmos.*, 91, 1089–1096, doi:10.1029/JD091iD01p01089, 1986b.

- Kelly, J. T., Baker, K. R., Nowak, J. B., Murphy, J. G., Markovic, M. Z., VandenBoer, T. C., Ellis, R. A., Neuman, J. A., Weber, R. J., Roberts, J. M., Veres, P. R., de Gouw, J. A., Beaver, M. R., Newman, S., and Misenis, C.: Fine-scale simulation of ammonium and nitrate over the South Coast Air Basin and San Joaquin Valley of California during CalNex-2010, *J. Geophys. Res.-Atmos.*, 119, 3600–3614, doi:10.1002/2013jd021290, 2014.
- Kroll, J. H. and Seinfeld, J. H.: Chemistry of secondary organic aerosol: formation and evolution of low-volatility organics in the atmosphere, *Atmos. Environ.*, 42, 3593–3624, doi:10.1016/j.atmosenv.2008.01.003, 2008.
- Macintyre, H. L. and Evans, M. J.: Sensitivity of a global model to the uptake of N₂O₅ by tropospheric aerosol, *Atmos. Chem. Phys.*, 10, 7409–7414, doi:10.5194/acp-10-7409-2010, 2010.
- Madronich, S.: Photodissociation in the atmosphere .1. Actinic flux and the effects of ground reflections and clouds, *J. Geophys. Res.-Atmos.*, 92, 9740–9752, doi:10.1029/JD092iD08p09740, 1987.
- Markovic, M. Z., VandenBoer, T. C., Baker, K. R., Kelly, J. T., and Murphy, J. G.: Measurements and modeling of the inorganic chemical composition of fine particulate matter and associated precursor gases in California's San Joaquin Valley during CalNex 2010, *J. Geophys. Res.-Atmos.*, 119, 6853–6866, doi:10.1002/2013JD021408, 2014.
- McDonald, B. C., Dallmann, T. R., Martin, E. W., and Harley, R. A.: Long-term trends in nitrogen oxide emissions from motor vehicles at national, state, and air basin scales, *J. Geophys. Res.-Atmos.*, 117, D00V18, doi:10.1029/2012jd018304, 2012.
- McNeill, V. F., Patterson, J., Wolfe, G. M., and Thornton, J. A.: The effect of varying levels of surfactant on the reactive uptake of N₂O₅ to aqueous aerosol, *Atmos. Chem. Phys.*, 6, 1635–1644, doi:10.5194/acp-6-1635-2006, 2006.
- Meyers, T. P., Huebert, B. J., and Hicks, B. B.: HNO₃ deposition to a deciduous forest, *Bound.-Lay. Meteorol.*, 49, 395–410, doi:10.1007/BF00123651, 1989.
- Munger, J. W., Jacob, D. J., Waldman, J. M., and Hoffmann, M. R.: Fogwater chemistry in an urban atmosphere, *J. Geophys. Res.-Oc. Atm.*, 88, 5109–5121, doi:10.1029/JC088iC09p05109, 1983.
- Murphy, J. G., Day, D. A., Cleary, P. A., Wooldridge, P. J., Millet, D. B., Goldstein, A. H., and Cohen, R. C.: The weekend effect within and downwind of Sacramento – Part 1: Observations of ozone, nitrogen oxides, and VOC reactivity, *Atmos. Chem. Phys.*, 7, 5327–5339, doi:10.5194/acp-7-5327-2007, 2007.
- Nelson, H. H. and Johnston, H. S.: Kinetics of the reaction of Cl with ClNO and ClNO₂ and the photochemistry of ClNO₂, *J. Phys. Chem.*, 85, 3891–3896, doi:10.1021/j150625a036, 1981.
- Nenes, A., Pandis, S., and Pilinis, C.: ISORROPIA: a new thermodynamic equilibrium model for multiphase multicomponent inorganic aerosols, *Aquat. Geochem.*, 4, 123–152, doi:10.1023/A:1009604003981, 1998.
- Ng, N. L., Kroll, J. H., Chan, A. W. H., Chhabra, P. S., Flagan, R. C., and Seinfeld, J. H.: Secondary organic aerosol formation from *m*-xylene, toluene, and benzene, *Atmos. Chem. Phys.*, 7, 3909–3922, doi:10.5194/acp-7-3909-2007, 2007.
- Pandis, S. N. and Seinfeld, J. H.: On the interaction between equilibration processes and wet or dry deposition, *Atmos. Environ. Part A – Gen.*, 24, 2313–2327, doi:10.1016/0960-1686(90)90325-H, 1990.
- Perring, A. E., Bertram, T. H., Wooldridge, P. J., Fried, A., Heikes, B. G., Dibb, J., Crouse, J. D., Wennberg, P. O., Blake, N. J., Blake, D. R., Brune, W. H., Singh, H. B., and Cohen, R. C.: Airborne observations of total RONO₂: new constraints on the yield and lifetime of isoprene nitrates, *Atmos. Chem. Phys.*, 9, 1451–1463, doi:10.5194/acp-9-1451-2009, 2009.
- Perring, A. E., Pusede, S. E., and Cohen, R. C.: An observational perspective on the atmospheric impacts of alkyl and multifunctional nitrates on ozone and secondary organic aerosol, *Chem. Rev.*, 113, 5848–5870, doi:10.1021/cr300520x, 2013.
- Pleim, J. E., Bash, J. O., Walker, J. T., and Cooter, E. J.: Development and evaluation of an ammonia bidirectional flux parameterization for air quality models, *J. Geophys. Res.-Atmos.*, 118, 3794–3806, doi:10.1002/jgrd.50262, 2013.
- Presto, A. A., Huff Hartz, K. E., and Donahue, N. M.: Secondary organic aerosol production from terpene ozonolysis. 2. Effect of NO_x concentration, *Environ. Sci. Technol.*, 39, 7046–7054, doi:10.1021/es050400s, 2005.
- Pusede, S. E. and Cohen, R. C.: On the observed response of ozone to NO_x and VOC reactivity reductions in San Joaquin Valley California 1995–present, *Atmos. Chem. Phys.*, 12, 8323–8339, doi:10.5194/acp-12-8323-2012, 2012.
- Pusede, S. E., Gentner, D. R., Wooldridge, P. J., Browne, E. C., Rollins, A. W., Min, K.-E., Russell, A. R., Thomas, J., Zhang, L., Brune, W. H., Henry, S. B., DiGangi, J. P., Keutsch, F. N., Harrold, S. A., Thornton, J. A., Beaver, M. R., St. Clair, J. M., Wennberg, P. O., Sanders, J., Ren, X., VandenBoer, T. C., Markovic, M. Z., Guha, A., Weber, R., Goldstein, A. H., and Cohen, R. C.: On the temperature dependence of organic reactivity, nitrogen oxides, ozone production, and the impact of emission controls in San Joaquin Valley, California, *Atmos. Chem. Phys.*, 14, 3373–3395, doi:10.5194/acp-14-3373-2014, 2014.
- Pusede, S. E., VandenBoer, T. C., Murphy, J. G., Markovic, M. Z., Young, C. J., Veres, P. R., Roberts, J. M., Washenfelder, R. A., Brown, S. S., Ren, X., Tsai, C., Stutz, J., Brune, W. H., Browne, E. C., Wooldridge, P. J., Graham, A. R., Weber, R., Goldstein, A. H., Dusanter, S., Griffith, S. M., Stevens, P. S., Lefer, B. L., and Cohen, R. C.: An atmospheric constraint on the NO₂ dependence of daytime near-surface nitrous acid (HONO), *Environ. Sci. Technol.*, 49, 12774–12781, doi:10.1021/acs.est.5b02511, 2015.
- Rollins, A. W., Browne, E. C., Min, K.-E., Pusede, S. E., Wooldridge, P. J., Gentner, D., Goldstein, A. H., Liu, S., Day, D. A., Russell, L. M., and Cohen, R. C.: Evidence for NO_x control over nighttime SOA formation, *Science*, 337, 1210–1212, doi:10.1126/science.1221520, 2012.
- Rood, M. J., Shaw, M. A., Larson, T. V., and Covert, D. S.: Ubiquitous nature of ambient metastable aerosol, *Nature*, 337, 537–539, doi:10.1038/337537a0, 1989.
- Russell, A. R., Valin, L. C., Bucsela, E. J., Wenig, M. O., and Cohen, R. C.: Space-based constraints on spatial and temporal patterns of NO_x emissions in California, 2005–2008, *Environ. Sci. Technol.*, 44, 3608–3615, doi:10.1021/es903451j, 2010.
- Russell, A. R., Perring, A. E., Valin, L. C., Bucsela, E. J., Browne, E. C., Wooldridge, P. J., and Cohen, R. C.: A high spatial resolution retrieval of NO₂ column densities from OMI: method and evaluation, *Atmos. Chem. Phys.*, 11, 8543–8554, doi:10.5194/acp-11-8543-2011, 2011.

- Russell, A. R., Valin, L. C., and Cohen, R. C.: Trends in OMI NO₂ observations over the United States: effects of emission control technology and the economic recession, *Atmos. Chem. Phys.*, 12, 12197–12209, doi:10.5194/acp-12-12197-2012, 2012.
- San Joaquin Valley Air Pollution Control Board, Rule 4901–Wood burning fireplaces and wood burning heaters: <http://www.valleyair.org/rules/currnrules/r4901.pdf> (last access: 5 January 2016), 2003.
- Schiferl, L. D., Heald, C. L., Nowak, J. B., Holloway, J. S., Neuman, J. A., Bahreini, R., Pollack, I. B., Ryerson, T. B., Wiedinmyer, C., and Murphy, J. G.: An investigation of ammonia and inorganic particulate matter in California during the CalNex campaign, *J. Geophys. Res.-Atmos.*, 119, 1883–1902, doi:10.1002/2013jd020765, 2014.
- Schmel, G. A.: Particle and gas dry deposition: a review, *Atmos. Environ.*, 14, 983–1011, doi:10.1016/0004-6981(80)90031-1, 1980.
- Shaw Jr., R. W., Stevens, R. K., Bowermaster, J., Tesch, J. W., and Tew, E.: Measurements of atmospheric nitrate and nitric acid: the denuder difference experiment, *Atmos. Environ.*, 16, 845–853, doi:10.1016/0004-6981(82)90403-6, 1982.
- Shaw, S. L., Mitloehner, F. M., Jackson, W., Depeters, E. J., Fadel, J. G., Robinson, P. H., Holzinger, R., and Goldstein, A. H.: Volatile organic compound emissions from dairy cows and their waste as measured by proton-transfer-reaction mass spectrometry, *Environ. Sci. Technol.*, 41, 1310–1316, doi:10.1021/es061475e, 2007.
- Sievering, H., Kelly, T., McConville, G., Seibold, C., and Turnipseed, A.: Nitric acid dry deposition to conifer forests: Niwot Ridge spruce-fir-pine study, *Atmos. Environ.*, 35, 3851–3859, doi:10.1016/S1352-2310(01)00156-X, 2001.
- Slinn, W. G. N.: Predictions for particle deposition to vegetative canopies, *Atmos. Environ.*, 16, 1785–1794, doi:10.1016/0004-6981(82)90271-2, 1982.
- Smith, T. B., Lehrman, D. E., Reible, D. D., and Shair, F. H.: The origin and fate of airborne pollutants within the San Joaquin Valley – volume 1, California Air Resources Board, Sacramento, California, 19 pp., 1981.
- Stolzenburg, M. R., Dutcher, D. D., Kirby, B. W., and Hering, S. V.: Automated measurement of the size and concentration of airborne particulate nitrate, *Aerosol Sci. Technol.*, 37, 537–546, doi:10.1080/02786820300922, 2003.
- Stull, R. B.: An Introduction to Boundary Layer Meteorology, 1st Edition, Atmospheric and Oceanographic Sciences Library, 13, Springer, the Netherlands, 1988.
- Stutz, J., Alicke, B., Ackermann, R., Geyer, A., Wang, S. H., White, A. B., Williams, E. J., Spicer, C. W., and Fast, J. D.: Relative humidity dependence of HONO chemistry in urban areas, *J. Geophys. Res.-Atmos.*, 109, D03307, doi:10.1029/2003jd004135, 2004.
- Thornton, J. A., Wooldridge, P. J., and Cohen, R. C.: Atmospheric NO₂: in situ laser-induced fluorescence detection at parts per trillion mixing ratios, *Anal. Chem.*, 72, 528–539, doi:10.1021/ac9908905, 1999.
- Thornton, J. A., Braban, C. F., and Abbatt, J. P. D.: N₂O₅ hydrolysis on sub-micron organic aerosols: the effect of relative humidity, particle phase, and particle size, *Phys. Chem. Chem. Phys.*, 5, 4593–4603, doi:10.1039/b307498f, 2003.
- Vayenas, D. V., Takahama, S., Davidson, C. I., and Pandis, S. N.: Simulation of the thermodynamics and removal processes in the sulfate-ammonia-nitric acid system during winter: implications for PM_{2.5} control strategies, *J. Geophys. Res.-Atmos.*, 110, D07S14, doi:10.1029/2004JD005038, 2005.
- Volpe Horii, C., William Munger, J., Wofsy, S. C., Zahniser, M., Nelson, D., and Barry McManus, J.: Atmospheric reactive nitrogen concentration and flux budgets at a Northeastern U.S. forest site, *Agr. Forest Meteorol.*, 133, 210–225, doi:10.1016/j.agrformet.2004.08.009, 2005.
- Wagner, N. L., Riedel, T. P., Young, C. J., Bahreini, R., Brock, C. A., Dube, W. P., Kim, S., Middlebrook, A. M., Ozturk, F., Roberts, J. M., Russo, R., Sive, B., Swarthout, R., Thornton, J. A., VandenBoer, T. C., Zhou, Y., and Brown, S. S.: N₂O₅ uptake coefficients and nocturnal NO₂ removal rates determined from ambient wintertime measurements, *J. Geophys. Res.-Atmos.*, 118, 9331–9350, doi:10.1002/jgrd.50653, 2013.
- Wahner, A., Mentel, T. F., Sohn, M., and Stier, J.: Heterogeneous reaction of N₂O₅ on sodium nitrate aerosol, *J. Geophys. Res.-Atmos.*, 103, 31103–31112, doi:10.1029/1998JD100022, 1998.
- Waldman, J. M., Munger, J. W., Jacob, D. J., Flagan, R. C., Morgan, J. J., and Hoffmann, M. R.: Chemical-composition of acid fog, *Science*, 218, 677–680, doi:10.1126/science.218.4573.677, 1982.
- Walker, J. M., Philip, S., Martin, R. V., and Seinfeld, J. H.: Simulation of nitrate, sulfate, and ammonium aerosols over the United States, *Atmos. Chem. Phys.*, 12, 11213–11227, doi:10.5194/acp-12-11213-2012, 2012.
- Watson, J. G., Chow, J. C., Bowen, J. L., Lowenthal, D. H., Hering, S., Ouchida, P., and Oslund, W.: Air quality measurements from the Fresno Supersite, *J. Air Waste Ma.*, 50, 1321–1334, doi:10.1080/10473289.2000.10464184, 2000.
- Weibring, P., Richter, D., Fried, A., Walega, J. G., and Dyroff, C.: Ultra-high-precision mid-IR spectrometer II: system description and spectroscopic performance, *Appl. Phys. B*, 85, 207–218, doi:10.1007/s00340-006-2300-4, 2006.
- Weibring, P., Richter, D., Walega, J. G., and Fried, A.: First demonstration of a high performance difference frequency spectrometer on airborne platforms, *Opt. Express*, 15, 13476–13495, doi:10.1364/OE.15.013476, 2007.
- Williams, E. J., Baumann, K., Roberts, J. M., Bertman, S. B., Norton, R. B., Fehsenfeld, F. C., Springston, S. R., Nunnermacker, L. J., Newman, L., Olszyna, K., Meagher, J., Hartsell, B., Edgerton, E., Pearson, J. R., and Rodgers, M. O.: Intercomparison of ground-based NO_y measurement techniques, *J. Geophys. Res.-Atmos.*, 103, 22261–22280, doi:10.1029/98JD00074, 1998.
- Winer, A. M., Peters, J. W., Smith, J. P., and Pitts, J. N.: Response of commercial chemiluminescent nitric oxide-nitrogen dioxide analyzers to other nitrogen-containing compounds, *Environ. Sci. Technol.*, 8, 1118–1121, doi:10.1021/es60098a004, 1974.
- Wooldridge, P. J., Perring, A. E., Bertram, T. H., Flocke, F. M., Roberts, J. M., Singh, H. B., Huey, L. G., Thornton, J. A., Wolfe, G. M., Murphy, J. G., Fry, J. L., Rollins, A. W., LaFranchi, B. W., and Cohen, R. C.: Total Peroxy Nitrates (ΣPNs) in the atmosphere: the Thermal Dissociation-Laser Induced Fluorescence (TD-LIF) technique and comparisons to speciated PAN measurements, *Atmos. Meas. Tech.*, 3, 593–607, doi:10.5194/amt-3-593-2010, 2010.

- Young, D. E., Kim, H., Parworth, C., Zhou, S., Zhang, X., Cappa, C. D., Seco, R., Kim, S., and Zhang, Q.: Influences of emission sources and meteorology on aerosol chemistry in a polluted urban environment: results from DISCOVER-AQ California, *Atmos. Chem. Phys. Discuss.*, 15, 35057–35115, doi:10.5194/acpd-15-35057-2015, 2015.
- Zhang, J., Chameides, W. L., Weber, R., Cass, G., Orsini, D., Edgerton, E., Jongejan, P., and Slanina, J.: An evaluation of the thermodynamic equilibrium assumption for fine particulate composition: nitrate and ammonium during the 1999 Atlanta Supersite Experiment, *J. Geophys. Res.*, 108, 8414, doi:10.1029/2001JD001592, 2003.
- Zhang, Y., Liu, P., Liu, X.-H., Pun, B., Seigneur, C., Jacobson, M. Z., and Wang, W.-X.: Fine scale modeling of wintertime aerosol mass, number, and size distributions in central California, *J. Geophys. Res.-Atmos.*, 115, D15207, doi:10.1029/2009jd012950, 2010.